JHEP05 (2014) 094

The mass-hierarchy and CP-violation discovery reach of the LBNO long-baseline neutrino experiment

The LAGUNA-LBNO collaboration

S.K. Agarwalla,[o] L. Agostino,[ag] M. Aittola,[z] A. Alekou,[h] B. Andrieu,[af] D. Angus,[w] F. Antoniou,[h] A. Ariga,[b] T. Ariga,[b] R. Asfandiyarov,[u] D. Autiero,[e] P. Ballett,[w] I. Bandac,[k] D. Banerjee,[a] G. J. Barker,[r] G. Barr,[s] W. Bartmann,[h] F. Bay,[a] V. Berardi,[aa] I. Bertram,[ad] O. Bésida,[k] A.M. Blebea-Apostu,[al] A. Blondel,[u] M. Bogomilov,[q] E. Borriello,[am] S. Boyd,[r] I. Brancus,[al] A. Bravar,[u] M. Buizza-Avanzini,[ag] F. Cafagna,[aa] M. Calin,[d] M. Calviani,[h] M. Campanelli,[aj] C. Cantini,[a] O. Caretta,[ae] G. Cata-Danil,[an] M.G. Catanesi,[aa] A. Cervera,[f] S. Chakraborty,[am] L. Chaussard,[e] D. Chesneanu,[al] F. Chipesiu,[al] G. Christodoulou,[t] J. Coleman,[t] P. Crivelli,[a] T. Davenne,[ae] J. Dawson,[ag] I. De Bonis,[ab] J. De Jong,[s] Y. Déclais,[e] P. Del Amo Sanchez,[ab] A. Delbart,[k] C. Densham,[ae] F. Di Lodovico,[g] S. Di Luise,[a] D. Duchesneau,[ab] J. Dumarchez,[af] I. Efthymiopoulos,[h] A. Eliseev,[ai] S. Emery,[k] K. Enqvist,[ac] T. Enqvist,[z] L. Epprecht,[a] A. Ereditato,[b] A.N. Erykalov,[ai] T. Esanu,[d] A.J. Finch,[ad] M.D. Fitton,[ae] D. Franco,[e] V. Galymov,[k] G. Gavrilov,[ai] A. Gendotti,[a] C. Giganti,[af] B. Goddard,[h] J.J. Gomez,[f] C.M. Gomoiu,[d,al] Y.A. Gornushkin,[j] P. Gorodetzky,[ag] N. Grant,[ad] A. Haesler,[u] M.D. Haigh,[r] T. Hasegawa,[an] S. Haug,[b] M. Hierholzer,[b] J. Hissa,[z] S. Horikawa,[a] K. Huitu,[ac] J. Ilic,[ae] A.N. Ioannisian,[x] A. Izmaylov,[i] A. Jipa,[d] K. Kainulainen,[n] T. Kalliokoski,[n] Y. Karadzhov,[u] J. Kawada,[b] M. Khabibullin,[i] A. Khotjantsev,[i] E. Kokko,[z] A.N. Kopylov,[i] L.L. Kormos,[ad] A. Korzenev,[u] S. Kosyanenko,[ai] I. Kreslo,[b] D. Kryn,[ag] Y. Kudenko,[i,l,m] V.A. Kudryavtsev,[c] J. Kumpulainen,[n] P. Kuusiniemi,[z] J. Lagoda,[p] I. Lazanu,[d] J.-M. Levy,[af] R.P. Litchfield,[r] K. Loo,[n] P. Loveridge,[ae] J. Maalampi,[n] L. Magaletti,[aa] R.M. Margineanu,[al] J. Marteau,[e] C. Martin-Mari,[u] V. Matveev,[i,j] K. Mavrokoridis,[t] E. Mazzucato,[k] N. McCauley,[t] A. Mercadante,[aa] O. Mineev,[i] A. Mirizzi,[am] B. Mitrica,[al] B. Morgan,[r] M. Murdoch,[t] S. Murphy,[a] K. Mursula,[z] S. Narita,[ao] D.A. Nesterenko,[ai] K. Nguyen,[a] K. Nikolics,[a] E. Noah,[u] Yu. Novikov,[ai] H. O'Keeffe,[ad] J. Odell,[ae] A. Oprima,[al] V. Palladino,[y] Y. Papaphilippou,[h] S. Pascoli,[w] T. Patzak,[ag,ah] D. Payne,[t] M. Pectu,[al] E. Pennacchio,[e] L. Periale,[a] H. Pessard,[ab] C. Pistillo,[b] B. Popov,[af,j] P. Przewlocki,[p] M. Quinto,[aa] E. Radicioni,[aa] Y. Ramachers,[r] P.N. Ratoff,[ad] M. Ravonel,[u] M. Rayner,[u] F. Resnati,[a] O. Ristea,[d]

A. Robert,[af] **E. Rondio,**[p] **A. Rubbia,**[a] **K. Rummukainen,**[ac] **R. Sacco,**[g] **A. Saftoiu,**[al]
K. Sakashita,[an] **J. Sarkamo,**[z] **F. Sato,**[an] **N. Saviano,**[am,w] **E. Scantamburlo,**[u]
F. Sergiampietri,[a,ap] **D. Sgalaberna,**[a] **E. Shaposhnikova,**[h] **M. Slupecki,**[z] **M. Sorel,**[f]
N.J.C. Spooner,[c] **A. Stahl,**[ak] **D. Stanca,**[al] **R. Steerenberg,**[h] **A.R. Sterian,**[al]
P. Sterian,[al] **B. Still,**[g] **S. Stoica,**[al] **T. Strauss,**[b] **J. Suhonen,**[n] **V. Suvorov,**[ai]
M. Szeptycka,[p] **R. Terri,**[g] **L.F. Thompson,**[c] **G. Toma,**[al] **A. Tonazzo,**[ag] **C. Touramanis,**[t]
W.H. Trzaska,[n] **R. Tsenov,**[q] **K. Tuominen,**[ac] **A. Vacheret,**[s] **M. Valram,**[al]
G. Vankova-Kirilova,[q] **F. Vanucci,**[ag] **G. Vasseur,**[k] **F. Velotti,** [h] **P. Velten,**[h] **T. Viant,**[a]
H. Vincke,[h] **A. Virtanen,**[n] **A. Vorobyev,**[ai] **D. Wark,**[ae] **A. Weber,**[s,ae] **M. Weber,**[b]
C. Wiebusch,[ak] **J.R. Wilson,**[g] **S. Wu,**[a] **N. Yershov,**[i] **J. Zalipska,**[p] **and M. Zito.**[k]

[a]*ETH Zurich, Institute for Particle Physics, Zurich, Switzerland*

[b]*University of Bern, Albert Einstein Center for Fundamental Physics,*
Laboratory for High Energy Physics (LHEP), Bern, Switzerland

[c]*Department of Physics and Astronomy, University of Sheffield, Sheffield, U.K.*

[d]*University of Bucharest, Faculty of Physics, Bucharest-Magurele, Romania*

[e]*Université de Lyon, Université Claude Bernard Lyon 1, IPN Lyon (IN2P3), Villeurbanne, France*

[f]*IFIC (CSIC & University of Valencia), Valencia, Spain*

[g]*Queen Mary University of London, School of Physics, London, U.K.*

[h]*CERN, Geneva, Switzerland*

[i]*Institute for Nuclear Research of the Russian Academy of Sciences, Moscow, Russia*

[j]*Joint Institute for Nuclear Research, Dubna, Moscow Region, Russia*

[k]*IRFU, CEA Saclay, Gif-sur-Yvette, France*

[l]*National Research Nuclear University "MEPhI", Moscow, Russia*

[m]*Moscow Institute of Physics and Technology, Moscow region, Russia*

[n]*Department of Physics, University of Jyväskylä, Jyväskylä, Finland*

[o]*Institute of Physics, Sachivalaya Marg, Sainik School Post, Bhubaneswar 751005, India*

[p]*National Centre for Nuclear Research (NCBJ), Warsaw, Poland*

[q]*Department of Atomic Physics, Faculty of Physics,*
St. Kliment Ohridski University of Sofia, Bulgaria

[r]*University of Warwick, Department of Physics, Coventry, U.K.*

[s]*Oxford University, Department of Physics, Oxford, U.K.*

[t]*University of Liverpool, Department of Physics, Liverpool, U.K.*

[u]*University of Geneva, section de Physique, DPNC, Geneva, Switzerland*

[w]*Institute for Particle Physics Phenomenology, Department of Physics, Durham University, U.K.*

[x]*Yerevan Physics Institute, Alikhanian Brothers Str. 2, Yerevan 0036, Armenia*

[y]*INFN Sezione di Napoli and Università di Napoli, Dipartimento di Fisica, Napoli, Italy*

[z]*Oulu Southern Institute and Department of Physics, University of Oulu, Oulu, Finland*

[aa]*INFN and Dipartimento interateneo di Fisica di Bari, Bari, Italy*

[ab]*LAPP, Université de Savoie, CNRS/IN2P3, F-74941 Annecy-le-Vieux, France*

[ac]*University of Helsinki, Helsinki, Finland*

[ad]*Physics Department, Lancaster University, Lancaster, U.K.*

[ae]*STFC, Rutherford Appleton Laboratory, Harwell Oxford, U.K.*

[af]*UPMC, Université Paris Diderot, CNRS/IN2P3, Laboratoire de Physique Nucléaire et de Hautes*
Energies (LPNHE), Paris, France

^{ag} APC, AstroParticule et Cosmologie, Université Paris Diderot, CNRS/IN2P3, CEA/Irfu,
   Observatoire de Paris, Sorbonne Paris Cité, 10,
   rue Alice Domon et Léonie Duquet, 75205 Paris Cedex 13, France

^{ah} Institut Universitaire de France, Maison des Universités 103,
   boulevard Saint-Michel 75005 Paris, France

^{ai} Petersburg Nuclear Physics Institute (PNPI), St-Petersburg, Russia

^{aj} Dept. of Physics and Astronomy, University College London, London, U.K.

^{ak} III. Physikalisches Institut, RWTH Aachen University, Aachen, Germany

^{al} Horia Hulubei National Institute of R&D for Physics and Nuclear Engineering,
   IFIN-HH, Romania

^{am} University of Hamburg, Hamburg, Germany

^{an} High Energy Accelerator Research Organization (KEK), Tsukuba, Ibaraki, Japan

^{ao} Iwate University, Department of Electrical Engineering and Computer Science,
   Morioka, Iwate, Japan

^{ap} INFN — Sezione di Pisa, Pisa, Italy

   E-mail: andre.rubbia@cern.ch

ABSTRACT: The next generation neutrino observatory proposed by the LBNO collaboration will address fundamental questions in particle and astroparticle physics. The experiment consists of a far detector, in its first stage a 20 kt LAr double phase TPC and a magnetised iron calorimeter, situated at 2300 km from CERN and a near detector based on a high-pressure argon gas TPC. The long baseline provides a unique opportunity to study neutrino flavour oscillations over their 1st and 2nd oscillation maxima exploring the L/E behaviour, and distinguishing effects arising from $\delta_{\rm CP}$ and matter.

In this paper we have reevaluated the physics potential of this setup for determining the mass hierarchy (MH) and discovering CP-violation (CPV), using a conventional neutrino beam from the CERN SPS with a power of 750 kW. We use conservative assumptions on the knowledge of oscillation parameter priors and systematic uncertainties. The impact of each systematic error and the precision of oscillation prior is shown. We demonstrate that the first stage of LBNO can determine unambiguously the MH to $> 5\sigma$ C.L. over the whole phase space. We show that the statistical treatment of the experiment is of very high importance, resulting in the conclusion that LBNO has $\sim 100\%$ probability to determine the MH in at most 4-5 years of running. Since the knowledge of MH is indispensable to extract $\delta_{\rm CP}$ from the data, the first LBNO phase can convincingly give evidence for CPV on the 3σ C.L. using today's knowledge on oscillation parameters and realistic assumptions on the systematic uncertainties.

Contents

1   Introduction

The main goals of the proposed LBNO [1] next-generation long-baseline neutrino and an-
tineutrino oscillation experiment are to discover CP-violation in the leptonic sector (CPV
or $\delta_{\rm CP} \neq 0$ and π) and determine the neutrino mass hierarchy (MH or $sign(\Delta m^2_{31}) = \pm 1$).
Discovery is defined according to usual practice in experimental high-energy physics as the
ability to exclude the wrong hypothesis with at least a 5σ confidence level (C.L.), while

a 3σ C.L. would correspond to an evidence for the tested hypothesis. Since propagation through Earth impacts neutrinos and antineutrinos differently, neutrino oscillations in matter can mimic a CP-asymmetry induced by $\delta_{\rm CP}$ and also affect the determination of the $\delta_{\rm CP}$ value. Hence, to decouple genuine CP-phase from matter induced effects, the strategy of LBNO is to exploit the L/E dependence of the $\nu_\mu \to \nu_e$ and $\bar\nu_\mu \to \bar\nu_e$ appearance probabilities with a wide-band beam at a baseline of 2300 km. Separate information on neutrinos and antineutrinos is obtained by changing the horn focusing polarity of the beam. The disappearance channels ($\nu_\mu \to \nu_\mu$ and $\bar\nu_\mu \to \bar\nu_\mu$) will constrain the atmospheric parameters and the muon charge identification will independently determine the $\nu_\mu/\bar\nu_\mu$ fluxes at the far distance. The $\nu_\mu \to \nu_\tau$ and $\bar\nu_\mu \to \bar\nu_\tau$ appearance channels will also be accessible with an unprecedented precision. Unlike the attempts of infering MH with atmospheric neutrinos, the accelerator-based approach of LBNO addresses both fundamental problems of CPV and MH in clean and straightforward conditions, profiting from the ability to reverse the focusing horns polarity and from the well-controlled fluxes, which characterise accelerator-based neutrino beams.

In this paper, we present an updated study of the sensitivity of LBNO, and discuss the impact of systematic errors and of the *a priori* knowledge of oscillation parameters. Following a realistic and incremental approach [2], the initial phase of LBNO foresees an underground $\sim$20 kton fiducial mass double-phase liquid Argon TPC complemented by a magnetised muon detector and coupled to a conventional neutrino beam from the CERN SPS, monitored by a magnetised near detector system. We show that this first realistic phase already provides conclusive and well-motivated physics opportunities. We employ a Monte-Carlo technique simulating a very large number of toy experiments to estimate the confidence level of the MH and CPV measurements. With the capability of reversing the horn focusing polarity, and even under pessimistic assumptions on systematic errors, a few years of running at the CERN SPS suffice for LBNO alone to produce a direct and guaranteed discovery of MH ($> 5\sigma$ C.L.) over the full phase space of oscillation parameters, and a unique sensitivity to CPV through the exploration of the first and second oscillation maxima. Neglecting any systematic error, LBNO in its first phase, has the power to reach a CPV discovery level $> 5\sigma$'s C.L., the actual significance depending on how far from zero and π the true value of $\delta_{\rm CP}$ is. The actually attainable CPV reach is sensitive to the prior knowledge of the oscillation parameters and to the achievable systematic errors on fluxes, cross-sections and detector-related effects. With conservative assumptions on the systematic errors and after $\sim$12 years of running at the CERN SPS, a significance for CPV above $> 3\sigma$'s C.L. will be reached for $\sim 25(40)\%$ of the $\delta_{\rm CP}$ values, under the expectation that $\sin^2 2\theta_{13}$ will be known from reactor experiments with a precision of $\pm 10(2.5)\%$. Several sources of systematic effects need to be addressed, in order to reduce the overall error balance and reach a discovery level. In particular, improvements in the present knowledge of the neutrino interaction differential cross-sections could increase the expected CPV discovery reach. Alternatively, a second phase of LBNO with an increased exposure with far more detector mass and beam power, aimed at reducing the statistical error around the 2nd oscillation maximum, would allow to reach a $> 5\sigma$ CPV discovery level over a wide range of $\delta_{\rm CP}$ values, even under the present conservative assumptions on systematic errors, thanks to the increased dependence on $\delta_{\rm CP}$ at the 2nd maximum.

2 Phenomenology for LBNO

The discovery that neutrinos change flavour while propagating in space — the phenomenon of *neutrino oscillations* — has historically been triggered by deep underground astrophysics experiments with neutrinos, first observing the Sun and, later on, the neutrinos generated in the interaction of cosmic rays with the Earth's atmosphere — the atmospheric neutrinos. At the same time the detection of a handful of neutrinos from the supernova SN1987A gave a fundamental input on astrophysical models. The firmly established flavour oscillations imply that neutrinos have small though non-vanishing and non-degenerate rest masses, and the existence of a physically observable mixing in the leptonic sector.

New physics is a key ingredient to resolve questions that the Standard Model (SM) cannot answer. In this context, neutrino masses and oscillations are, to this day, the only experimentally established Beyond the Standard Model (BSM) physics. In the framework of three neutrino family scenario, the weak eigenstates ν_α ($\alpha = $ e,μ,τ) are given as linear combinations of the mass eigenstates ν_i (of definite mass m_i, i=1,2,3) via the Pontecorvo-Maki-Nakagawa-Sakata (PMNS) [3, 4] matrix U as $\nu_\alpha = \sum_i U_{\alpha i} \nu_i$. The 3×3 unitary matrix U is generally parameterized by the three mixing angles θ_{12}, θ_{13}, θ_{23}, and the phase $\delta_{\rm CP}$ (where we have neglected Majorana phases):

$$U = \begin{pmatrix} U_{e1} & U_{e2} & U_{e3} \\ U_{\mu1} & U_{\mu2} & U_{\mu3} \\ U_{\tau1} & U_{\tau2} & U_{\tau3} \end{pmatrix} = \begin{pmatrix} 1 & 0 & 0 \\ 0 & c_{23} & s_{23} \\ 0 & -s_{23} & c_{23} \end{pmatrix} \begin{pmatrix} c_{13} & 0 & s_{13}e^{-i\delta} \\ 0 & 1 & 0 \\ -s_{13}e^{i\delta} & 0 & c_{13} \end{pmatrix} \begin{pmatrix} c_{12} & s_{12} & 0 \\ -s_{12} & c_{12} & 0 \\ 0 & 0 & 1 \end{pmatrix} \quad (2.1)$$

where c_{ij} and s_{ij} represent $\cos(\theta_{ij})$ and $\sin(\theta_{ij})$, respectively. The parameter $\delta_{\rm CP}$ is the phase that controls the CP asymmetry.

The present level of understanding of the PMNS matrix already represents an incredible experimental achievement, which will culminate in the determination of the phase $\delta_{\rm CP}$. Global analyses [5–8] of all neutrino oscillation data, including the recent highest precision measurements, indicate that the "minimal" three-neutrino PMNS framework is sufficient to completely describe the observed oscillation phenomenology (apart from some "anomalies" in terrestrial short baseline experiments). The question of the CP-violation in the leptonic sector (CPV) remains an unresolved and urgent problem of particle physics. All data are self-consistent and are compatible with any value for $\delta_{\rm CP}$ in $0 \leq \delta_{\rm CP} \leq 2\pi$ within the 2σ confidence range.

The neutrino mass hierarchy (MH) or the sign of $\Delta m_{31}^2 \equiv m_3^2 - m_1^2$ is also not yet known: whether m_3 is the heaviest mass eigenvalue (normal hierarchy, $\Delta m_{31}^2 > 0$) or m_3 is the lightest one (inverted hierarchy, $\Delta m_{31}^2 < 0$) remains to be experimentally determined, and presently there is no evidence indicating a preference for either value. Such an experimental determination is a crucial ingredient to resolve the problem of CPV. It is also relevant for the understanding of the origin of neutrino masses, which is expected to relate to BSM physics. In particular, an inverted hierarchy would be a strong hint that some unexpected physics is underlying the masses and flavour problem, and an important ingredient for leptogenesis scenarios. The mass hierarchy is important to interpret cosmological observations probing the hot dark matter fraction. Likewise, future data from supernova bursts will be more

easily interpreted with the MH known. Finally, the existence of an inverted mass hierarchy would be an useful input for neutrino-less double beta decay searches, which aim at testing the Majorana nature of neutrinos (see e.g. [9]).

Both CPV and MH problems can be addressed with accelerator-based long-baseline neutrino oscillation experiments via the electron appearance channels $\nu_\mu \to \nu_e$ and $\bar{\nu}_\mu \to \bar{\nu}_e$. Including higher order terms and the effect of coherent forward scattering pointed out by Wolfenstein in case of neutrino oscillations in matter [10], the $\nu_\mu \to \nu_e$ oscillation probability can be approximated as [11]:

$$
\begin{aligned}
P(\nu_\mu \to \nu_e) \simeq\ & 4c_{13}^2 s_{13}^2 s_{23}^2 \left\{ 1 + \frac{a}{\Delta m_{31}^2} \cdot 2(1 - 2s_{13}^2) \right\} \sin^2 \frac{\Delta m_{31}^2 L}{4E} \\
& + c_{13}^2 s_{13} s_{23} \left\{ -\frac{aL}{E} s_{13} s_{23}(1 - 2s_{13}^2) \right. \\
& \left. \qquad\qquad + \frac{\Delta m_{21}^2 L}{E} s_{12}(-s_{13} s_{23} s_{12} + c_\delta c_{23} c_{12}) \right\} \sin \frac{\Delta m_{31}^2 L}{2E} \\
& - 4\frac{\Delta m_{21}^2 L}{2E} s_\delta c_{13}^2 s_{13} c_{23} s_{23} c_{12} s_{12} \sin^2 \frac{\Delta m_{31}^2 L}{4E}
\end{aligned}
\tag{2.2}
$$

where $c_{ij} = \cos\theta_{ij}$, $s_{ij} = \sin\theta_{ij}$, $c_\delta = \cos\delta_{\rm CP}$, $s_\delta = \sin\delta_{\rm CP}$, and $a = 2\sqrt{2}G_F n_e E$, with n_e representing the electron density of the traversed medium. The corresponding probability for $\bar{\nu}_\mu \to \bar{\nu}_e$ transition is obtained by replacing $\delta_{\rm CP} \to -\delta_{\rm CP}$ and $a \to -a$. The CP-violating effects of $\delta_{\rm CP}$ are modulated by those of all three mixing angles and their interplay, resulting in complicated dependencies and leading to an *a priori* eight-fold parameter degeneracy [12]. In addition, coherent forward scattering in matter affects oscillations, and also produces an asymmetry between neutrinos and anti-neutrinos.

Several ideas have emerged worldwide in order to advance the field, and have converged into rather well defined projects such as LBNO [1], LBNE [13] and Hyper-Kamiokande [14]. A general consensus, reflected in the above mentioned setups, is that new generation very large scale and deep underground neutrino detectors will be needed to satisfactorily address open questions such as CPV and MH. In this context, it is handy to define two asymmetries between the probability of oscillations of neutrinos and antineutrinos, one related to the CP effect computed in vacuum $\mathcal{A}_{\rm CP}^{\rm vac}(\delta_{\rm CP})$:

$$
\mathcal{A}_{\rm CP}^{\rm vac}(\delta_{\rm CP}) \equiv \left(\frac{P^{\rm vac}(\nu) - P^{\rm vac}(\bar{\nu})}{P^{\rm vac}(\nu) + P^{\rm vac}(\bar{\nu})} \right)
\tag{2.3}
$$

and the other to the matter effects $\mathcal{A}_{\rm CP}(\rho)$ computed in matter for a fixed value of $\delta_{\rm CP}$:

$$
\mathcal{A}_{\rm CP}(\rho) \equiv \left(\frac{P^{mat}(\nu) - P^{mat}(\bar{\nu})}{P^{mat}(\nu) + P^{mat}(\bar{\nu})} \right)
\tag{2.4}
$$

where ρ represents the traversed Earth matter density (in the constant density approximation). These two variables, plotted in the two dimensional plane of the neutrino energy E_ν versus the baseline L, are shown in figure 1. In these graphs, the black regions correspond to combinations of neutrino energy and baseline at which the oscillation phenomena is
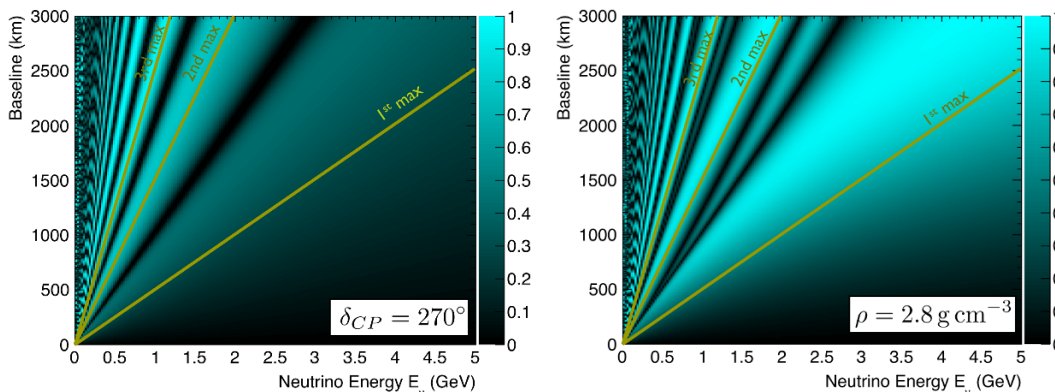
Figure 1: The asymmetries, $abs(\mathcal{A}_{\mathrm{CP}}^{\mathrm{vac}}(\delta_{CP}))$ and $abs(\mathcal{A}_{\mathrm{CP}}(\rho))$ (as defined eqs. (2.3) and (2.4)) in the (E_ν, L) plane. (left panel) CP asymmetry in vacuum for $\delta_{\mathrm{CP}} = 270°$. (right panel): matter asymmetry for a given Earth density and with $\delta_{\mathrm{CP}} = 0°$. The 1st, 2nd and 3rd oscillation maxima are represented by yellow lines at constant L/E_ν's.

insensitive to the effect, while the light (blueish) regions correspond to those where the effect is largest.

These features lead to the following phenomenological observations, which were taken into account in the definition of the LBNO experimental setup:

- The CP asymmetries increase from the first to higher orders oscillation maxima. This is understood by the fact that $\mathcal{A}_{\mathrm{CP}}^{\mathrm{vac}}(\delta_{\mathrm{CP}})$ has an envelope determined by [11]:

$$\frac{2 s_\delta c_{12} s_{12}}{s_{13}} \cot\theta_{23} \frac{\Delta m_{21}^2 L}{2E} \tag{2.5}$$

  which grows as L/E. The 2nd maximum is hence more sensitive to CPV than the 1st maximum. Hence, access to the 2nd maxima extends the sensitivity to CPV, in particular when the measurement at the first maximum becomes systematic dominated.

- A large matter asymmetry is visible in a broad energy region just below the first maximum.

- The energy dependence of the probability can resolve several parameter degeneracies, and allows in particular disentangling the CP-driven and the matter-driven effects, if the baseline is large enough.

- Conversely, if the mass hierarchy is unknown, or if the matter effects are treated as a source of systematic error, degeneracies reduce the ability to significantly detect CPV.

- Assuming an energy threshold of about $1\,\mathrm{GeV}$, which is a realistic value taking into account on-axis conventional neutrino beam fluxes from high energy protons, and the vanishing neutrino cross-sections at low energies (in particular for antineutrinos), the measurement of the 2nd maximum requires a baseline greater than 1500 km:

$$E_\nu^{\mathrm{2nd\,max}} \gtrsim 1\,\mathrm{GeV} \Longrightarrow \mathrm{L} \gtrsim 1500 \text{ km} \tag{2.6}$$

In order to attack the challenging problem of CPV and the related MH determination, LBNO adopts a combination of methods, by precisely measuring the disappearance and appearance energy spectrum shapes (in particular, peak position and height for 1st and 2nd oscillation maximum and minimum) with high resolution, and by comparing neutrino- and antineutrino-induced oscillations. The liquid Argon and magnetized iron detectors will in fact provide complementary studies of all three active transitions $\nu_\mu \to \nu_\mu$, $\nu_\mu \to \nu_e$ and $\nu_\mu \to \nu_\tau$ charged current events over the optimized range of neutrino energies. They can also probe the active-sterile transition with neutral current events. A precise investigation of the oscillation probabilities as a function of energy and a comparison of neutrino and antineutrino behaviours will verify if they follow the expectations from 3-generation neutrino mixing.

As will be exposed in this paper, LBNO is optimised to best perform these measurements and yields a definitive resolution of MH and a significant exploration of CPV. The goal of the near detectors will be to precisely predict the unoscillated neutrino fluxes, using well-developed and tested techniques in present long-baseline experiments, such as T2K [15]. Hadro-production and neutrino cross-section campaigns will cover the relevant region for LBNO. The 2300 km baseline is adequate to have an excellent separation of the asymmetry due to the matter effects (i.e. the mass hierarchy measurement) and the CP asymmetry due to the $\delta_{\rm CP}$ phase, and thus to break the parameter degeneracies. Therefore, the existence of matter and CP-violation induced effects will be examined without over-relying on theoretical modelling and assumptions, and the standard neutrino paradigm will be tested explicitly. Hence, the LBNO approach to extract MH and $\delta_{\rm CP}$ value is clean and straightforward.

3 The LBNO experimental setup — An incremental approach

As today's state-of-art is set by the Super-Kamiokande detector (SK) with its 22.5 kton fiducial mass, new detectors should be more than an order of magnitude larger than SK or use technologies which can outperform the Water Cherenkov technique, such as the liquid Argon (LAr) Time Projection Chamber [16]. Taking into account the latest knowledge of oscillation parameters, the construction feasibility of such a large underground laboratory, the detector itself and the involved costs, the LBNO Expression of Interest [1] proposes *an incremental approach* at the Pyhäsalmi mine. The incremental approach is motivated by physics, technical and financial aspects. From the point of view of oscillation physics, the priority for the underground far detectors is the initial 20 kton double phase LAr LEM-TPC (GLACIER [17, 18]) combined with a magnetized muon detector (MIND [19, 20]) in one of two large underground caverns (see ref. [1] for details). Schematic views of a 20 kton LAr detector and a 35 kt MIND detector are shown in figure 2. In the current engineering concept, the 20 kton LAr detector has a total LAr mass of 32.5 kton, and an instrumented active mass of 22.8 kton [1]. In the simulations performed for this paper, the field cage of the 20 kton detector is approximated with a cylinder of radius 33 m and height 20 m, corresponding to an instrumented volume of 17100 m^3 and an active mass of 23.9 kton.

LBNO builds upon the results of several years of design studies funded by the European Commission (EC). LAGUNA was organized as a 3-years long project, to carry
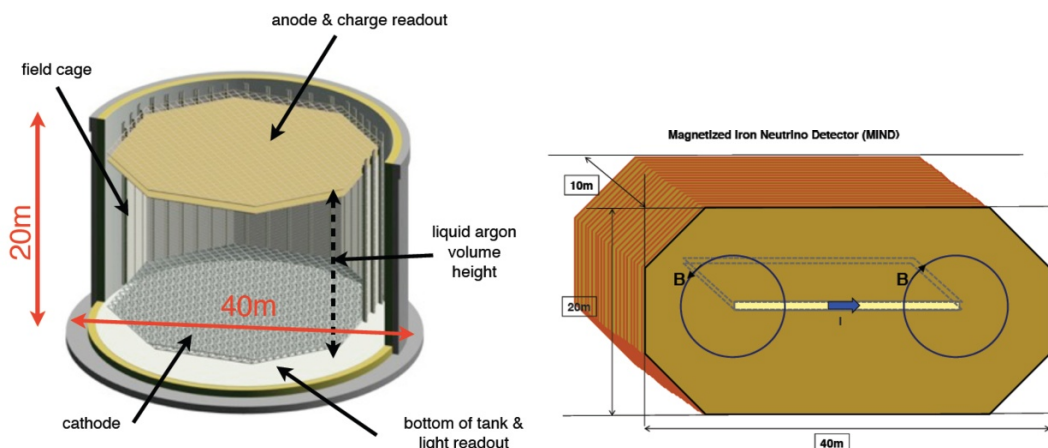
Figure 2: Schematic view of the 20 kt LAr detector (left panel) and the 35 kt MIND detector (right panel).

out underground sites investigations and develop a concept for a facility able to host the new underground neutrino observatory. It was primarily motivated by the fact that, although Europe currently has four national underground laboratories (at Boulby (UK), Canfranc (Spain), Gran Sasso (Italy), and Modane (France)), none of them is large enough to host a next-generation observatory. LAGUNA selected seven potential underground sites (Boulby (UK), Canfranc (Spain), Fréjus (France), Pyhäsalmi (Finland), Sieroczow-ice (Poland), Slanic (Romania), Umbria (Italy)) to study, and compared them in order to identify the scientifically and technically most appropriate and cost-effective strategy towards a large scale European neutrino observatory. One of the key conclusion of LA-GUNA is that all of the seven considered underground sites are *in principle* technically feasible, and able to host the desired types of detectors. With the reduced impact of all the other factors, site selection should be based on physics arguments. A second phase called LAGUNA-LBNO has been funded by the EC and initiated in October 2011. It further evaluated the findings of LAGUNA, and in particular, it assessed the underground construction of the large detectors, their commissioning, and the long-term operation of the facility. LAGUNA-LBNO is in addition specifically considering long-baseline beams from CERN [21]. From the seven pre-selected LAGUNA sites, the two deepest, Fréjus (overburden of 4800 m.w.e.) and Pyhäsalmi (overburden of 4000 m.w.e.), were found particularly attractive and retained further attention. Careful simulations and a detailed analysis of the key findings of LAGUNA have motivated the choice of the CERN-Pyhäsalmi baseline (2300 km) *as the first priority*. Two main physics criteria were considered in order to optimize the choice of the site, informed by the first indications of large θ_{13} [22], which have since then being strongly confirmed by reactors [23] and T2K [24, 25].

4 The LBNO physics programme

For long-baseline physics in the post-θ_{13} discovery era, the LAr and magnetized iron detectors provide complementary studies of the three active transitions $\nu_\mu \to \nu_\mu$, $\nu_\mu \to \nu_e$ and

$\nu_\mu \to \nu_\tau$ charged current events over a range of neutrino energies optimized via tuning of the conventional beam focusing, and can also probe the active-sterile transition by measuring neutral current events. A precise investigation of the oscillation probabilities as a function of energy and a comparison of neutrino and antineutrino behaviours will verify if they follow the expectations from 3-generation neutrino mixing. The 2300 km baseline is optimised to break the parameter degeneracies and provide a definitive resolution of MH and a significant exploration of CPV in the neutrino sector.

The chosen location in one of the deepest mine in Europe ($\sim$ 4000 m.w.e.) will also provide a unique opportunity to observe very rare phenomena with a LAr detector, independent of the CERN beam events. Proton decay can be explored in many different — often background free — decay channels. After 10 years of exposure, the sensitivity on the proton lifetime will reach $\tau_p \geq 2 \times 10^{34}$ years at 90% C.L. in the $p \to K\bar{\nu}$ channel. In addition, other exclusive decay channels will be investigated, such as $p \to e^+\pi^0$ and $p \to \mu^+\pi^0$. Measuring many different channels helps to distinguish between models. Furthermore, 5600 atmospheric neutrino events per year will be measured. Atmospheric neutrinos, detected with good energy- and angular resolution and flavor identification are a new tool to perform oscillation physics complementary to the CERN beam, and could be a new method to obtain a radiography of the Earth's interior via matter effects. The neutrino burst from a galactic supernova (SN) explosion would be observed with high statistics in the electron neutrino channel, providing invaluable information on the inner mechanism of the SN explosion and on neutrino oscillations, not accessible to other setups. For a supernova explosion at 10 kpc, $\sim$ 10,000 neutrino interactions will be recorded in the active LAr volume. Unknown sources of astrophysical neutrinos, like for instance those that could arise from annihilation processes of WIMP particles in astrophysical objects could also be observed.

5   New CERN beam layout

The beam under design is a conventional third generation neutrino beam facility based on the CNGS [26] technology. Initially, the facility will use protons from an upgraded CERN SPS accelerator, reaching 750 kW of nominal beam power. This high-intensity operation goes beyond the record intensity of 565 kW ever achieved in the SPS [27], and 60% above the operational beam power for CNGS. The main limitations to achieve such intensities come from beam losses in both PS and SPS, and due to limited RF power at SPS. In table 1 the expectations for the SPS potential in delivering intense beams for a future neutrino program are described, coming as stretched goal within the foreseen LHC injector upgrades (LIU) project [28]. Table 2 summarises the key parameters for the beam. The quoted yearly intensities correspond to 200 days of running mode with 80% efficiency for the accelerators, and $60 \div 85\%$ of beam sharing with other users for the case of SPS.

To profit from existing infrastructures for the target hall and near detector, in the baseline option, the LBNO beam could be located near the SPS North Area as shown in figure 3. Under this hypothesis, for the first stage using the 400 GeV from SPS, the primary beam would be extracted from the TT2 channel and transported for about 400 m in the

	CNGS	RECORD	LBNO
E_{SPS} [GeV]	400	400	400
Bunch spacing [ns]	5	5	5
I_{bunch} [$\times 10^{10}$]	1.05	1.3	1.7
N_{bunches}	4200	4200	4200
I_{SPS} [$\times 10^{13}$]	4.4	5.3	7.0
I_{PS} [$\times 10^{13}$]	2.3	3.0	4.0
PS cycle length [s]	1.2	1.2	1.2/2.4
SPS cycle length [s]	6.0	6.0	6.0/7.2
E_{PS} [GeV/c]	14	14	14
Beam power [kW]	470	565	747/622

Table 1:   Present, All-time Record, and Possible Future SPS Parameters for Neutrino Type Beams.

Parameter	SPS beam	HP-PS beam
$E_{\mathrm{beam}}[GeV]$	400	$50 \div 75$
$I_{\mathrm{beam}}[ppp]$	7×10^{13}	$2.5 \div 1.7 \times 10^{14}$
Cycle length [s]	6	1
$P_{\mathrm{beam}}[MW]$	0.750	2
$\mathrm{POT}_{\mathrm{year}}$ [10^{21}]	$0.10 \div 0.14$	$3.46 \div 2.35$

Table 2:   Key parameters of the assumed LBNO proton beam from the SPS and HP-PS [29].

existing TT20 line. Then it would branch off to a new 480 m long transfer line required to match the direction and more importantly create the 10.4° downward slope required to point to the far detector. For the fast extraction from SPS in the Long Straight section-2 (LSS2), a novel scheme was developed to bypass the lack of space to install new kickers in the region whilst maintaining the elements required for the slow extraction to fixed-target experiments. The new scheme uses a non local extraction combining kickers in LSS6 and LSS2 sections. First tests with beam have shown encouraging results, further studies are planned after the restart of the CERN accelerators in 2015 [30].

A key constraint in the location and design of the secondary beam comes from the steep 18.1% slope required due to the long-baseline. The combination of high-intensity and high beam energy put a constraint on the minimum distance between the target and the near detector location to ensure that the high-energy muons are absorbed in the beam dump and the earth, preventing them from generating background in the near detector. Considering the first phase with the primary beam at 400 GeV and assuming a rock density of 2.3 g/cm^3, preliminary Monte Carlo calculations suggest that a distance of at least 800 m is necessary if a passive concrete shielding of about 100 m long is used in the beam dump. As a consequence, the near detector cavern will be 144 m deeper than the target. Therefore, the option to branch off from the TT20 line at its upmost point very close to the surface is

Figure 3: The baseline layout for the LBNO neutrino facility in the vicinity of the CERN North Area.

very attractive, as it allows the whole installation to be at smaller depths with significant cost savings. In this configuration the target cavern is located at -41 m, the hadron stop at -100 m and the near detector at -185 m, almost at the same level as the deepest point of LHC.

Three upgrade scenarios are being considered for the neutrino beam. These primarily involve upgrade or alternative scenarios for the proton injector to the same target area beyond the initial operation with the present SPS: (i) use of an upgraded high-energy PS or SPS, machines discussed in the HE-LHC option, (ii) use of a new dedicated HP-PS synchrotron [29], (iii) use of a Neutrino Factory beam concept. The prospects for a major upgrade of the LBNO neutrino beam are very attractive, offering a long term vision. The realization of the HP-PS accelerator with MW power would expand the capability of the LBNO facility and provide an interesting way to increase the exposure by a significant factor without prohibitively extending the running time. The chosen baseline of 2300 km is suitable to implement a Neutrino Factory, opening the path towards an ultimate exploration and an era of high-precision oscillation studies.

6 Beam optimisation and expected raw event rates

The neutrino beamline design is a central component of the LBNO optimisation, since it will directly impact the long-baseline physics reach, affecting for instance the mass hierarchy sensitivity, the CP violation reach and the study of the other oscillation channels like the tau neutrino appearance. Different beamline designs have been investigated and a preliminary design has been established in an effort to illustrate the compelling physics reach of the experiment.
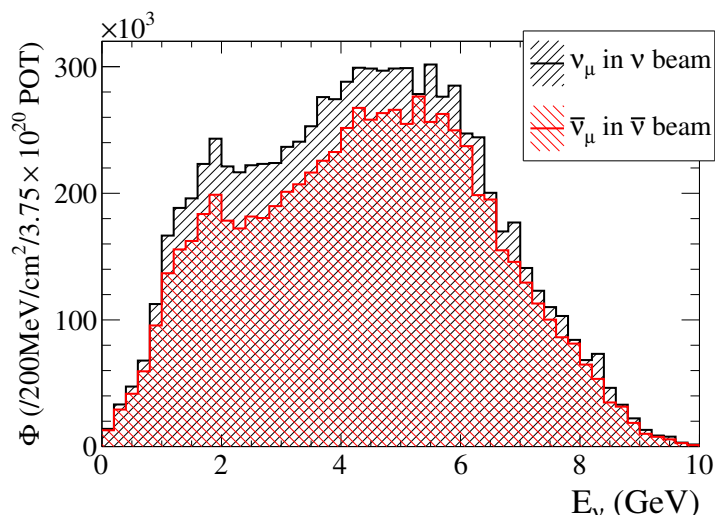
Figure 4: Neutrino and anti-neutrino flux for the CERN to Pyhäsalmi beam.

The neutrino beam line is tentatively composed of a target, two horns and a decay volume. The target is modelled as a 1 m long cylinder of graphite with density $\rho = 1.85$ g/cm^3 and 2 mm radius. The focusing system is based on a pair of parabolic horns which we will denote as horn (upstream) and reflector (downstream) according to the current terminology. The decay tunnel is 300 m long and 3 m wide. A new beam optimisation is currently under way to investigate different possible beam optics, which should lead to enhanced rates and an optimised beam profile for the LBNO physics program. A further optimisation of the decay tunnel could also increase the neutrino flux. The unoscillated neutrino and anti-neutrino beam flux is shown in figure 4.

The expected charged (CC) and neutral current (NC) interaction rates are computed using the optimisation of the focusing optics for 400 GeV and are shown in table 3. The rates under the assumption of the potential 2nd phase at 2 MW with the new HP-PS 50 GeV are listed in table 4 for completeness. The oscillated rates are computed using the oscillation parameters from the global fit of ref. [8]. The NC interactions rate are for events with visible energy > 0.5 GeV. The rate is given for an exposure of 50 kt.yrs, so 2.5 years with the 20 kton baseline LAr detector.

For comparison, the rates for LBNE with the baseline of 1300 km are also shown and normalised to the same exposure. The parameters and flux of the LBNE beam correspond to those described in ref. [31].

Although the LBNE baseline of 1300 km is significantly shorter than the LBNO baseline of 2300 km, the expected rate of oscillated events in both setups are very similar, in both neutrino and antineutrino mode. This is explained by the fact that the longer baseline requires also higher energy neutrinos in order to keep the L/E parameter of both setups around the atmospheric region. The resulting higher boost of the parent mesons, and the resulting higher neutrino energies, compensate for the increase distance, by making the beam more pencil-like and profiting from the linearly increasing total neutrino interaction cross-section.

Beam	ν_μ unosc. CC	ν_μ osc. CC	ν_e beam CC	ν_μ NC	$\nu_\mu \to \nu_\tau$ CC	$\nu_\mu \to \nu_e$ CC $\delta_{\rm CP} = -\pi/2$,	0,	$\pi/2$
LBNO: 2300 km NH 400 GeV, 750 kW 1.5×10^{20} POT/year								
50kt years ν	3447	907	22	1183	215	246	201	162
50kt years $\bar{\nu}$	1284	330	5	543	98	20	27	29
LBNO: 2300 km IH 400 GeV, 750 kW 1.5×10^{20} POT/year								
50kt years ν	3447	853	22	1183	239	71	43	32
50kt years $\bar{\nu}$	1284	330	5	543	99	61	77	89
LBNE Low energy beam 120 GeV, 700 kW, NH 6×10^{20} POT/year								
50kt years ν	4882	1765	44	1513	61	217	174	126
50kt years $\bar{\nu}$	2506	890	13	620	22	44	54	56
LBNE Low energy beam 120 GeV, 700 kW, IH 6×10^{20} POT/year								
50kt years ν	4882	1713	44	1513	67	120	82	58
50kt years $\bar{\nu}$	2506	875	13	620	23	59	69	82

Table 3: Raw ν oscillation event rates at the far site with $E_\nu < 10$ GeV normalised to 50kt years, corresponding to 2.5 years of data-taking with the 20 kton baseline LAr detector. See text.

Beam	ν_μ unosc. CC	ν_μ osc. CC	ν_e beam CC	ν_μ NC	$\nu_\mu \to \nu_\tau$ CC	$\nu_\mu \to \nu_e$ CC $\delta_{\rm CP} = -\pi/2$,	0,	$\pi/2$
LBNO: 2300 km NH 50 GeV, 2 MW 3.0×10^{21} POT/year								
50kt years ν	8616	2266	54	2955	539	615	502	406
50kt years $\bar{\nu}$	3325	828	13	1360	249	44	65	73
LBNO: 2300 km IH 50 GeV, 2 MW 3.0×10^{21} POT/year								
50kt years ν	8616	2132	54	2955	596	177	109	79
50kt years $\bar{\nu}$	3325	828	13	1360	249	154	192	224

Table 4: Same as table 3 but under the assumption of the HP-PS 50 GeV accelerator at 2 MW operation. These rates are shown for completeness, they are not used in the calculations shown in this paper.
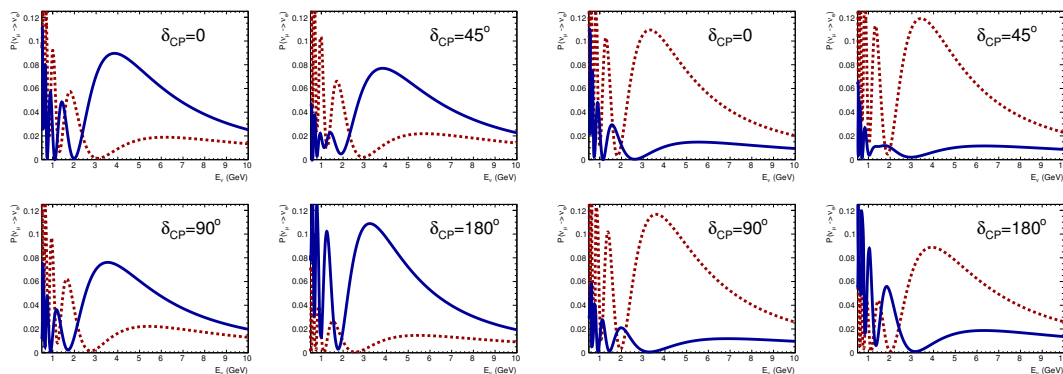
Figure 5: Oscillation probability of $\nu_\mu \to \nu_e$ (blue) and $\bar{\nu}_\mu \to \bar{\nu}_e$ (red-dashed) for different values of δ_{cp} for (left) normal hierarchy $\Delta m_{31}^2 > 0$ (NH), (right) inverted hierarchy $\Delta m_{31}^2 < 0$ (IH), and $\sin^2 2\theta_{13} = 0.09$. The spectral information provides an unambiguous determination of the oscillation parameters and allows in principle to distinguish the two CP-conserving scenarios, namely $\delta_{CP} = 0$ and $\delta_{CP} = \pi$.

7 Mass hierarchy and CP violation measurements at LBNO

7.1 General principle

Our primary goal is to determine the mass hierarchy and measure CP violation by observing ν_μ to ν_e oscillations, through a precise measurement of the neutrino spectrum and the comparison of neutrino- and antineutrino-induced oscillations. The 2300 km baseline is adequate to have an excellent separation of the asymmetry due to the matter effects (i.e. the mass hierarchy measurement) and the CP asymmetry due to the δ_{CP} phase, and thus to break the parameter degeneracies. The probabilities of $\nu_\mu \to \nu_e$ and $\bar{\nu}_\mu \to \bar{\nu}_e$ oscillations contain the spectral information which provides an unambiguous determination of the oscillations parameters and allows discriminating between the two CP-conserving scenarios, namely $\delta_{CP} = 0$ and $\delta_{CP} = \pi$.

Once the distance between source and detector is fixed, the oscillatory behaviour of the neutrino flavour conversion can be easily translated to that for the expected neutrino energy spectrum of the oscillated events. If the neutrino energy spectrum of the oscillated events can be reconstructed with sufficiently good resolution in order to distinguish first and second maxima, the spectral information obtained is invaluable for the unambiguous determination of the oscillation parameters.

The probabilities of $\nu_\mu \to \nu_e$ and $\bar{\nu}_\mu \to \bar{\nu}_e$ oscillations for $\sin^2 2\theta_{13} = 0.09$ and different values of δ_{CP} and normal hierarchy (NH) and inverted hierarchy (IH) are shown in figure 5, as they are expected in LBNO at the 2300 km baseline. The plots illustrate qualitatively that the spectral information provides an unambiguous determination of the oscillation parameters and allows discriminating between the two CP-conserving scenarios. The δ_{CP}-phase and matter effects introduce a well-defined energy dependence of the oscillation probability. As a consequence, the neutrino energy spectrum of the oscillated events need to be experimentally reconstructed with sufficiently good resolution in order to distin-

guish first and second maximum, and extract unambiguous information on the oscillation parameters. Using these signals, it is also possible to test the standard 3-neutrino mixing framework, by looking for deviations from the expected L/E dependence and by comparing neutrinos and antineutrinos. For instance, neutrino decays and neutrino decoherence effects, due to the coupling to the environment, could lead to damping in the amplitude of the oscillations at large L/E; non-standard interactions, due to new neutrino interactions, can lead to a modification of matter effects with a suppression of the conversion probability at high energy and a change of the resonance energy, if they are sufficiently strong; CPT and/or Lorentz violating effects can produce a markedly different behaviour for neutrinos and antineutrinos and specific L/E signatures, especially at low energy.

At the same time, the matter effects at 2300 km are large and the NH and IH scenarios induce to an almost complete swap of behaviours between neutrinos and antineutrinos. This is clearly exhibited in figure 5. Hence, CP- and matter-induced asymmetries are very different and distinguishable.

A sample of electron-like (e-like) events is thus a primary source of information. We consider the following background contributions to the signal e-like events:

- Intrinsic ν_e contamination present in the beam (intrinsic ν_e),

- Electron events from ν_τ charged current interaction with subsequent leptonic τ decay ($\nu_\tau \to e$ contamination),

- Neutral current ν_μ events with π^0 production (NCπ^0),

- Mis-identified muons from ν_μ CC interactions (mis-id ν_μ).

In addition, we use μ-like events in the disappearance channel ($\nu_\mu \to \nu_\mu$ survival probability) to constrain the atmospheric oscillation parameters, Δm_{31}^2 and $\sin^2 \theta_{23}$. A detailed description of neutrino event simulations and selection efficiency can be found in ref. [1].

7.2 Experimental observables

We use reconstructed neutrino energy $E_\nu^{\rm rec}$ and missing momentum in the transverse plane, defined by the incoming neutrino beam direction, $p_T^{\rm miss}$ of each e-like event to construct bi-dimensional distributions useful to discriminate signal from background. Examples of such distributions are shown in figure 6 for a value of $\delta_{\rm CP} = 0$ and the case of normal mass hierarchy. As can be seen in the figure, the shapes of signal and background contributions in the $E_\nu^{\rm rec} - p_T^{\rm miss}$ phase-space differ. In particular, NC π^0 interactions are characterized by low $E_\nu^{\rm rec}$ values, while events originating from ν_τ CC interactions tend to have larger $p_T^{\rm miss}$ than the ν_e CC events because of the two neutrinos in the final state. This allows a better signal-background discrimination against neutral currents and tau charged current events, than if one were to use $E_\nu^{\rm rec}$ information only. In the future, a cut-based or neural network analysis could be employed to further improve the purity of the e-like sample. In the case of the μ-like events, only the reconstructed neutrino energy is used, since backgrounds are less severe.
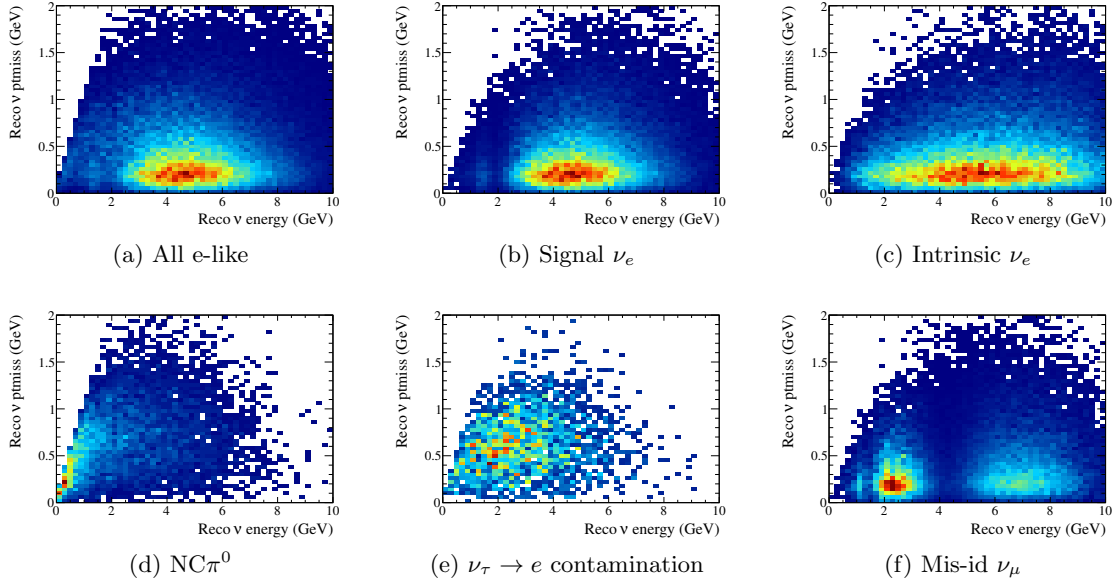
Figure 6: Example event distributions for various channels contributing to the e-like sample for $\delta_{\text{CP}} = 0$ and the case of the normal mass hierarchy.

7.3 Analysis method

To evaluate the physics potential of the experiment it is mandatory do develop a sophisticated analysis package, which takes into account all the available experimental information and the sources of systematic uncertainties. The LBNO collaboration has developed such specific tools.

We perform a fit of the oscillation parameters by minimizing the following χ^2 with respect to the oscillation parameters $\mathbf{o}$ that are not fixed and systematic parameters $\mathbf{f}$ (tables 5 and 6):

$$\chi^2 = \chi^2_{\text{appear}} + \chi^2_{\text{disa}} + \chi^2_{\text{syst}}. \tag{7.1}$$

The χ^2_{appear} is the term corresponding to the electron appearance. It is given by:

$$\chi^2_{\text{appear}} = 2 \sum_{+/-} \sum_{E_\nu^{\text{rec}}, p_T^{\text{miss}}} n_e(E_\nu^{\text{rec}}, p_T^{\text{miss}}; \mathbf{o}_{\text{test}}, \mathbf{f}_{\text{test}}) - n_e(E_\nu^{\text{rec}}, p_T^{\text{miss}}; \mathbf{o}_{\text{true}}, \mathbf{f}_{\text{true}})$$
$$+ n_e(E_\nu^{\text{rec}}, p_T^{\text{miss}}; \mathbf{o}_{\text{true}}, \mathbf{f}_{\text{true}}) \ln \frac{n_e(E_\nu^{\text{rec}}, p_T^{\text{miss}}; \mathbf{o}_{\text{true}}, \mathbf{f}_{\text{true}})}{n_e(E_\nu^{\text{rec}}, p_T^{\text{miss}}; \mathbf{o}_{\text{test}}, \mathbf{f}_{\text{test}})}, \tag{7.2}$$

where the subscript true (test) refers to the true (test) values of the $\mathbf{o}$ and $\mathbf{f}$ parameters. The true parameters are those chosen by Nature, while test refer to the parameter at which we compute the likelihood with respect to the true value. The first sum in eq. (7.2) corresponds to adding the contributions from the neutrino and anti-neutrino beam running.

The number of the e-like events in a given $E_\nu^{\mathrm{rec}} - p_T^{\mathrm{miss}}$ bin is determined according to:

$$
\begin{aligned}
n_e(E_\nu^{\mathrm{rec}}, p_T^{\mathrm{miss}}; \mathbf{o}, \mathbf{f}) = {} & f_{\mathrm{sig}} n_{e-sig}(E_\nu^{\mathrm{rec}}, p_T^{\mathrm{miss}}; \mathbf{o}) \\
& + f_{\nu_e} n_{\nu_e}(E_\nu^{\mathrm{rec}}, p_T^{\mathrm{miss}}; \mathbf{o}) + f_{\nu_\tau} n_{e,\nu_\tau}(E_\nu^{\mathrm{rec}}, p_T^{\mathrm{miss}}; \mathbf{o}) \\
& + f_{\mathrm{NC}}(n_{\mathrm{NC}\pi^0}(E_\nu^{\mathrm{rec}}, p_T^{\mathrm{miss}}; \mathbf{o}) + n_{\mathrm{mis}-\nu_\mu}(E_\nu^{\mathrm{rec}}, p_T^{\mathrm{miss}}; \mathbf{o})),
\end{aligned}
\tag{7.3}
$$

where n_{e-sig}, n_{ν_e}, n_{e,ν_τ}, $n_{\mathrm{NC}\pi^0}$, and $n_{\mathrm{mis}-\nu_\mu}$ are the number of events for signal, intrinsic beam ν_e, electrons from tau decay, neutral current, and mis-identified ν_μ, respectively.

The information from the disappearance channel is contained in the χ^2_{disa} term of total χ^2 in eq. (7.1), which is given by

$$
\begin{aligned}
\chi^2_{\mathrm{disa}} = 2 \sum_{+/-} \sum_{E_\nu^{\mathrm{rec}}} & n_\mu(E_\nu^{\mathrm{rec}}; \mathbf{o}_{\mathrm{test}}, \mathbf{f}_{\mathrm{test}}) - n_\mu(E_\nu^{\mathrm{rec}}; \mathbf{o}_{\mathrm{true}}, \mathbf{f}_{\mathrm{true}}) \\
& + n_\mu(E_\nu^{\mathrm{rec}}; \mathbf{o}_{\mathrm{true}}, \mathbf{f}_{\mathrm{true}}) \ln \frac{n_\mu(E_\nu^{\mathrm{rec}}; \mathbf{o}_{\mathrm{true}}, \mathbf{f}_{\mathrm{true}})}{n_\mu(E_\nu^{\mathrm{rec}}; \mathbf{o}_{\mathrm{test}}, \mathbf{f}_{\mathrm{test}})}.
\end{aligned}
\tag{7.4}
$$

The number of μ-like events is the sum of signal ($n_{\mu-sig}$) and $\tau \to \mu$ background (n_{μ,ν_τ}) contributions and is calculated as

$$
n_\mu(E_\nu^{\mathrm{rec}}; \mathbf{o}, \mathbf{f}) = f_{\mathrm{sig}} n_{\mu-sig}(E_\nu^{\mathrm{rec}}; \mathbf{o}) + f_{\nu_\tau} n_{\mu,\nu_\tau}(E_\nu^{\mathrm{rec}}; \mathbf{o}).
\tag{7.5}
$$

The oscillation and the systematic parameters are constrained through the χ^2_{syst} term:

$$
\chi^2_{\mathrm{syst}} = \sum_i \frac{(a_{0,i} - a_i)^2}{\sigma^2_{a_i}},
\tag{7.6}
$$

where $a_{0,i}$ (a_i) is the prior (test) value of the ith parameter and σ_{a_i} is the corresponding prior uncertainty. As will be shown in section 7.5, we use 6 priors for the neutrino oscillation parameters, and 4 for the normalisation uncertainties of signal and background.

In order to study the sensitivity of LBNO to CP violation, we define a test statistic $\Delta\chi^2$

$$
\Delta\chi^2 = \chi^2_{\delta_{\mathrm{CP}}} - \chi^2_{\mathrm{best}},
\tag{7.7}
$$

where $\chi^2_{\delta_{\mathrm{CP}}}$ is the minimized χ^2 of eq. (7.1) at a fixed value of δ_{CP} (true or test), while χ^2_{best} is the minimum χ^2 obtained when δ_{CP} is allowed to vary over the full range of possible values.

To evaluate sensitivity of the experiment to MH, we define the following test statistic T:

$$
T = \chi^2_{\mathrm{IH}} - \chi^2_{\mathrm{NH}}
\tag{7.8}
$$

where χ^2_{IH} (χ^2_{NH}) is obtained by minimizing the χ^2 of eq. (7.1), marginalising with respect to systematic and oscillation parameters (including δ_{CP}) around the negative (positive) Δm^2_{31}. The value of T depends on δ_{CP}.

The statistical method to determine MH and CPV is described in detail in the next section.

7.4 Statistical approach to MH and CPV determination

The sensitivity of an experiment to MH and CPV can be defined using the frequentist approach to the test of simple hypothesis, which we will review briefly.

The aim is to establish a criterion to assess that a "null hypothesis" H_0 is considered true and that an "alternative hypothesis" H_1 can be rejected. One chooses a test statistic T that will be computed from the experimental data. This quantity is a stochastic variable with a certain probability density function (PDF) which should be different whether H_0 or H_1 is true. One then defines a "critical region" such that, when T has values within this region, H_0 is accepted as the true hypothesis. The probability to obtain a value of T outside the critical region and consequently to reject H_0 even though it is true ("type I" error or "loss") is usually denoted as α. The confidence level (CL) with which one accepts H_0 as true is therefore

$$CL = 1 - \alpha. \tag{7.9}$$

In addition, one must also consider the probability that H_0 is accepted as true even though H_1 is true ("type II" error or "contamination"). This probability is usually denoted as β. The power of the test p, namely the probability of rejecting H_0 when it is false, is then

$$p = 1 - \beta. \tag{7.10}$$

To calculate the CL and the power of the test, one has to know the respective PDFs of T for H_0 and H_1. It has recently been pointed out [32, 33] that for the case of MH and T as in eq. (7.8), the PDF can be approximated by a Gaussian whose width is related to its mean $\pm|T_0|$ as $\sigma = \sqrt{2|T_0|}$. Since in general the values of $|T_0|$ for NH and IH could be different, one has

$$
\begin{aligned}
PDF(T|NH) &= N\left(|T_0^{\mathrm{NH}}|, \sqrt{2|T_0^{\mathrm{NH}}|}\,\right) \\
PDF(T|IH) &= N\left(-|T_0^{\mathrm{IH}}|, \sqrt{2|T_0^{\mathrm{IH}}|}\,\right).
\end{aligned}
\tag{7.11}
$$

For the long baseline oscillation experiments whose sensitivity comes primarily from the electron appearance channel, $|T_0^{\mathrm{NH}}|$ and $|T_0^{\mathrm{IH}}|$ also have a strong dependency on the presently unknown CPV phase δ_{CP}. We assume that also in the future MH will be determined without precise knowledge on δ_{CP}, hence study the problem as a function of the assumed true value of δ_{CP}.

To verify that eqs. (7.11) are applicable for the LBNO case, we generated 20,000 toy data samples for different exposures, several values of δ_{CP}, and both hierarchy cases. Each data sample was then analyzed and T was calculated according to eq. (7.8). The distributions of T values for NH and IH obtained assuming $\delta_{\mathrm{CP}} = \pi/2$ and a total exposure of 2.25×10^{20} POT ($50\%\nu : 50\%\bar{\nu}$ running), or about two years of data taking, are shown in the left panel of figure 7. Each distribution is fitted with a Gaussian function to determine the mean T_0 and the width σ_T. The right panel of figure 7 shows the ratio of $\sigma_T/\sqrt{T_0}$ as a function of T_0. As can be seen, the results from toy distributions deviate in some cases from the $\sigma_T = 2\sqrt{T_0}$ rule. The effect of these deviations is, however, expected to be small and therefore we will subsequently assume that PDF for T is given by eqs. (7.11).
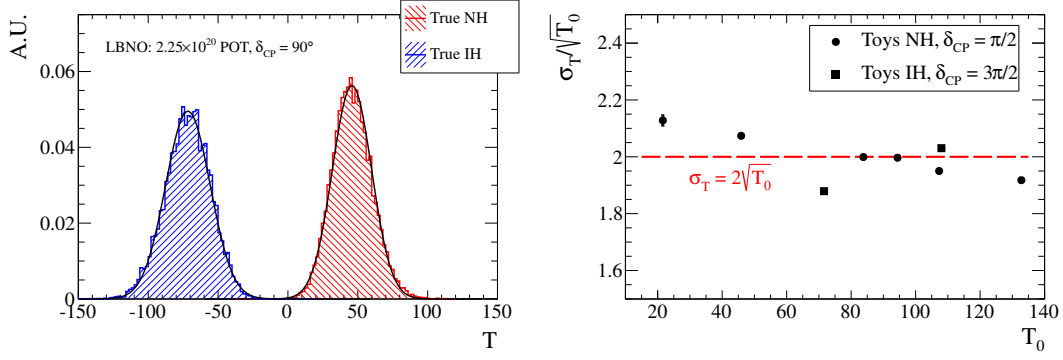
Figure 7: Distribution of the T test statistic for NH and IH for an exposure of 2.25×10^{20} POT (or approx. 2 years of running) and $\delta_{\rm CP} = \pi/2$ (left) and width of the distributions as a function of the average value T_0 (right).

To present the statistical treatment in the case of the MH determination, we begin by considering NH as our H_0. If one wants to achieve a given CL for determining of the MH, we should consider values of T larger than a given critical value as suggesting NH to be true. We should thus define a critical value T_C^α, depending on the corresponding α, such that

$$1 - \alpha = \int_{T_C^\alpha}^{\infty} PDF(T|\text{NH}) \, dT \tag{7.12}$$

gives a desired CL. The power of the test is given by

$$p = 1 - \beta = 1 - \int_{-\infty}^{T_C^\alpha} PDF(T|\text{IH}) \, dT. \tag{7.13}$$

The procedure is formally similar for IH as H_0.

As pointed out in [34], if the PDFs of T follow the distributions of equation (7.11), the critical value and the power become simple analytically functions of the chosen α. For the case $H_0 = $ NH, we have

$$T_C^\alpha = T_0^{\rm NH} - \sqrt{8 T_0^{\rm NH}} \cdot \text{Erfc}^{-1}(2\alpha) \tag{7.14}$$

and

$$p = 1 - \beta = 1 - \frac{1}{2} \text{Erfc}\left(\frac{T_0^{\rm IH} + T_C^\alpha}{\sqrt{8 T_0^{\rm IH}}} \right) \qquad \text{(for MH)}. \tag{7.15}$$

The calculation must be repeated for the case $H_0 = $ IH, with $T_0^{\rm NH}$ and $T_0^{\rm IH}$ interchanged.

The values of $T_0^{\rm NH}$ and $T_0^{\rm IH}$ depend on the unknown $\delta_{\rm CP}$. As explained in [34], one should therefore set T_C^α in the most pessimistic case, i.e. for the smallest absolute value of T_0 in either case. As shown later, this corresponds to choosing $T_0^{\rm NH}$ ($T_0^{\rm IH}$) for $\delta_{\rm CP} = \pi/2$ ($\delta_{\rm CP} = 3\pi/2$). We thus compute T_C^α as

$$\begin{aligned} T_C^\alpha(T_0^{\rm NH}(\delta_{\rm CP} = \pi/2)) & \qquad \text{for } H_0 = \text{NH}, \\ T_C^\alpha(T_0^{\rm IH}(\delta_{\rm CP} = 3\pi/2)) & \qquad \text{for } H_0 = \text{IH}. \end{aligned} \tag{7.16}$$

– 18 –
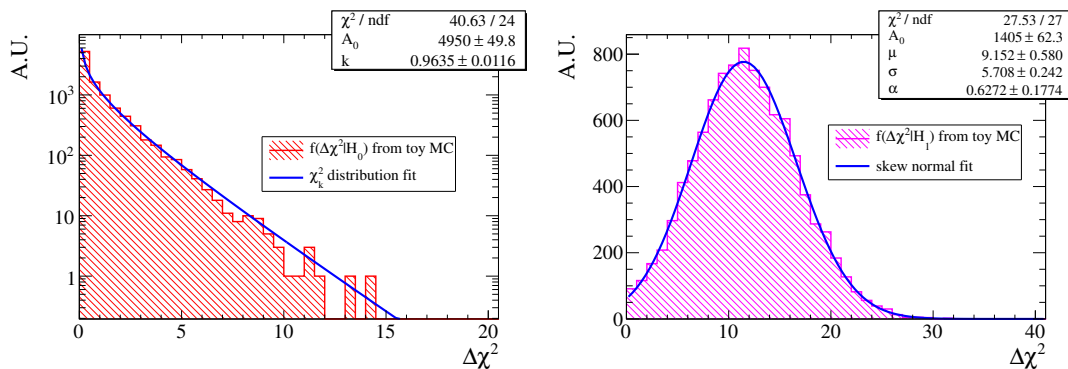
Figure 8: Distribution of the $\Delta\chi^2$ test statistic for $\delta_{\rm CP} = 0$ (left) and $\delta_{\rm CP} = \pi/2$ (right) for an exposure of 15×10^{20} POT.

Once T_C^α is fixed, the statistical power will be a function of $\delta_{\rm CP}$. For the test of NH, it will be largest for $\delta_{\rm CP} = \pi/2$ and smallest for $\delta_{\rm CP} = 3\pi/2$ (where $T_0^{\rm IH}$ is smallest), while the opposite is true for IH.

A similar approach was used to study the $\delta_{\rm CP}$ phase determination. In this case, H_0 corresponds to $\delta_{\rm CP} = 0$ or π and H_1 to $0 < \delta_{\rm CP} < 2\pi$ (both hypotheses are composite). We are in the case of "nested hypotheses". The distribution of the $\Delta\chi^2$ test statistic computed according to eq. (7.7) follows a χ^2 distribution with 1 d.o.f. when the null hypothesis is true, as shown in figure 8(left), and is independent of the exposure. In the case of the alternative hypothesis, the distribution, shown in figure 8(right) for the case of $\delta_{\rm CP} = \pi/2$, is obtained using toy Monte Carlo simulations. To construct it, we generate toy data samples assuming the true values for $\delta_{\rm CP}$ of 0 and π. We then compute the $\Delta\chi^2$ statistic as defined in eq. (7.7) for a given test value of $\delta_{\rm CP}$ for both cases, i.e,

$$\Delta\chi_0^2 = \chi^2(\delta_{\rm CP}^{\rm test}|\delta_{\rm CP}^{\rm true} = 0) - \chi_{\rm best}^2(|\delta_{\rm CP}^{\rm true} = 0)$$
$$\Delta\chi_\pi^2 = \chi^2(\delta_{\rm CP}^{\rm test}|\delta_{\rm CP}^{\rm true} = \pi) - \chi_{\rm best}^2(|\delta_{\rm CP}^{\rm true} = \pi). \tag{7.17}$$

Finally, we take the smallest of the two $\Delta\chi^2$s:

$$\Delta\chi^2 = \min{(\Delta\chi_0^2, \Delta\chi_\pi^2)}. \tag{7.18}$$

For computational purposes we approximate the resultant distribution analytically with a skew normal distribution. It should be noted that the average of this distribution defines the sensitivity for a given value of $\delta_{\rm CP} \neq 0, \pi$ and this is the quantity that will be shown in the figures of section 9.

Hence, for the CPV discovery, the null hypothesis will be accepted at a given CL when the value of $\Delta\chi^2$ is below a critical computed from the quantiles of the $\chi^2(1 \text{ d.o.f.})$ distribution. The power of the test is the integral of the skew normal distribution above the critical value.

7.5 Assumption on parameters and systematics

Assumptions on the oscillation parameters and uncertainties as well as on the beam line characteristics are shown in table 5. Values take into account the results from ongoing

Name	Value	error (1σ)	error (%)
L	2300 km	exact	exact
Δm_{21}^2	$7.6 \times 10^{-5}\ eV^2$	exact	exact
$|\Delta m_{31}^2| \times 10^{-3}\ eV^2$	2.420	± 0.091	± 3.75 %
$\sin^2 \theta_{12}$	0.31	exact	exact
$\sin^2 2\theta_{13}$	0.10	± 0.01	$\pm 10\%$
$\sin^2 \theta_{23}$	0.440	± 0.044	$\pm 10\%$
Average density of traversed matter (ρ)	3.20 g/cm^3	± 0.13	$\pm 4\%$

Table 5: Assumptions on the values of the oscillation parameters and their uncertainties.

Name	Value	error (1σ)
Signal normalization (f_{sig})	1	$\pm 5\%$
Beam electron contamination normalization (f_{ν_e})	1	$\pm 5\%$
Tau normalization (f_{ν_τ})	1	$\pm 20\% - \pm 50\%$
ν NC and ν_μ CC background (f_{NC})	1	$\pm 10\%$

Table 6: Assumptions on event normalization uncertainties (bin-to-bin correlated errors).

experiments, in particular reactor experiments, and are based on the global analyses published in the literature [6–8]. Uncertainties are given at 1σ and in percent. We have chosen to use the values available as of today, therefore our assumptions are conservative. Concerning the value of θ_{23}, we assume the first octant solution for all the sensitivity studies. Nevertheless, since a second octant solution is not excluded at present, we will take into account the effect of varying θ_{23} between the two octants on the MH and CP sensitivity (See section 8 and 9.3.2).

In order to describe matter effects, we use a constant average density approximation. We have compared the analytical oscillation probability obtained with the constant value to the one computed by integration of the oscillation amplitude in 50 steps through the Earth described by the Preliminary reference earth model (PREM) [35]. As can be seen in figure 9, the assumed value of 3.20 g/cm^3 describes best the probability computed with the PREM. In the figure, the band corresponds to the oscillation probabilities obtained by varying the density in the interval $3.2 > \rho > 2.8$ g/cm^3. The upper values of the band are found for $\rho = 3.20$ g/cm^3.

The assumptions on systematic errors on signal and background normalization are shown in table 6. The systematic error on the tau normalization is set to 50% for the mass hierarchy determination and to 20% for the δ_{CP} sensitivity studies. This reduction is due to the fact that the experiment will be able to constrain ν_τ cross section with the data accumulated during first few years of running performing specific tau neutrino appearance channel measurements to constrain the production rate.

These errors are assumed to be fully correlated among the energy bins.
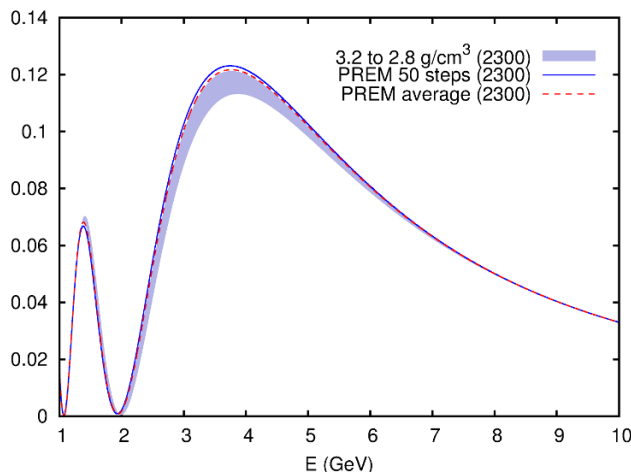
Figure 9: Oscillation $\nu_\mu \to \nu_e$ probability along the CERN-Pyhäsalmi baseline for (1) fixed average matter density varying on the interval $3.2 > \rho > 2.8$ g/cm^3, (2) PREM 50 steps (3) PREM average. In the band, the upper values correspond to a density of 3.2 g/cm^3.
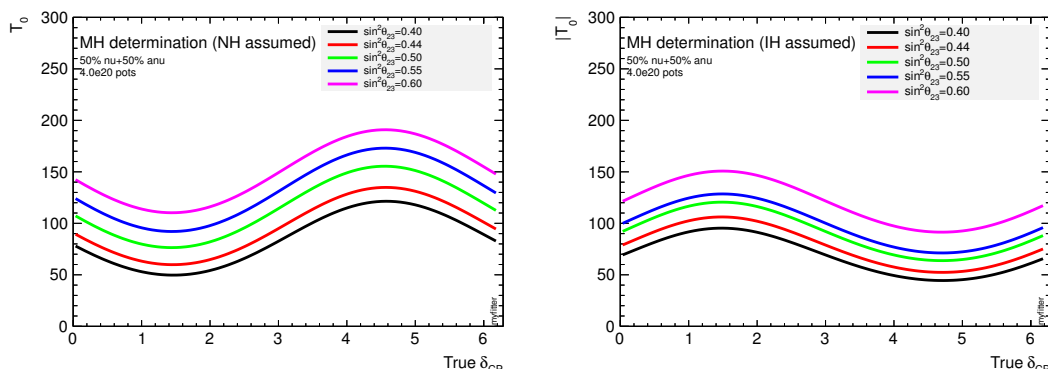
Figure 10: Mean value of the mass hierarchy test statistic as a function of true $\delta_{\rm CP}$ for a total exposure of 4×10^{20} pots (or about 4 years of running at the SPS) and LBNO 20 kton detector. Left: normal Hierarchy assumed. Right: inverted Hierarchy assumed.

8 Mass Hierarchy determination

Mass hierarchy sensitivity studies have been developed using a 50% ν 50% $\bar{\nu}$ sharing, which is optimised for this measurement, and 4×10^{20} POT, corresponding to about 4 years of nominal data taking with the SPS at 750 kW. The mean value T_0 of the test statistic T defined in eq. (7.8) for mass hierarchy determination is shown in figure 10 as a function of $\delta_{\rm CP}$, for the assumed Normal and Inverted true mass hierarchy. The parameter with the largest impact on the matter oscillation probabilities, and thus on the mass hierarchy determination, is the θ_{23} mixing angle. Figure 10 shows also the effect of varying θ_{23} by a large amount in the two octants. This study proves that the present uncertainty on θ_{23} does not compromise the sensitivity of our experiment. The other sources of uncertainty considered above can only have a smaller impact.
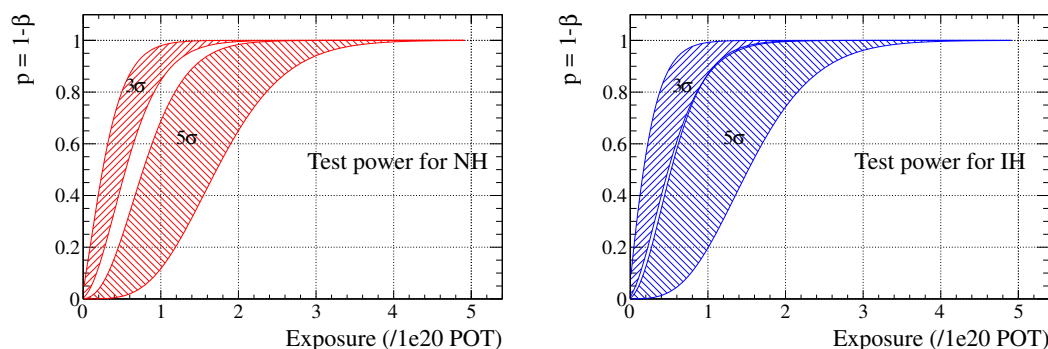
Figure 11: Statistical power as a function of exposure for the test of NH (left) and IH (right) for 3σ and 5σ CL. The nominal central values for oscillation parameters have been assumed and the shaded bands correspond to the variation of $\delta_{\rm CP}$.

Following the statistical method discussed in section 7.4, the power of LBNO for NH and the IH determination at a confidence level of 3σ or 5σ is shown in figure 11 as a function of exposure. The shaded area corresponds to the variation of $\delta_{\rm CP}$ and the extreme values are reached for $\delta_{\rm CP} = \pi/2$ or $3\pi/2$, as has been explained above. One can see that LBNO has a probability of essentially 100% to discover the MH in either case for any value of $\delta_{\rm CP}$. An exposure of slightly more that 2×10^{20}pot will guarantee that a 3σ CL is obtained, while a 5σ CL will be reached with less than 4×10^{20}pot, corresponding to about 4 years of SPS running.

9 Study of the sensitivity to CP violation

9.1 Beam focusing mode optimisation

For the CP phase measurement, the beam normalisation is set to $1.5\,10^{21}$ protons on target (POT) (or approximately 12 years of nominal running at the SPS), and the optimisation of the beam sharing between ν and $\bar{\nu}$ has been studied in detail. Figure 12 shows the sensitivities for a non vanishing $\delta_{\rm CP}$ for the two mass hierarchies assuming different percentage of sharing assuming all the parameters in table 5 and 6. Our simulations show a maximum of coverage in the case of 75 % ν - 25% $\bar{\nu}$. This sharing will be assumed for all the studies presented in the next paragraphs.

9.2 Significance of a first and second maxima analysis method

The analysis method takes into account the information contained in the whole shape of the e-like event distributions in both the ranges of the 1$^{\rm st}$ and the 2$^{\rm nd}$ oscillation maximum. To consider both the oscillation maxima as well as the spectral shape is a very powerful method to extract $\delta_{\rm CP}$ and to confirm the oscillatory behaviour predicted in the three neutrino oscillation schema together with matter effects. This approach is the only one proposed to put in evidence the theoretical framework of oscillations as a whole. In fact, the spectrum shape as well as the number of events strongly depend on the value of $\delta_{\rm CP}$ in particular in the energy region corresponding to the 2$^{\rm nd}$ maximum. We have compared the
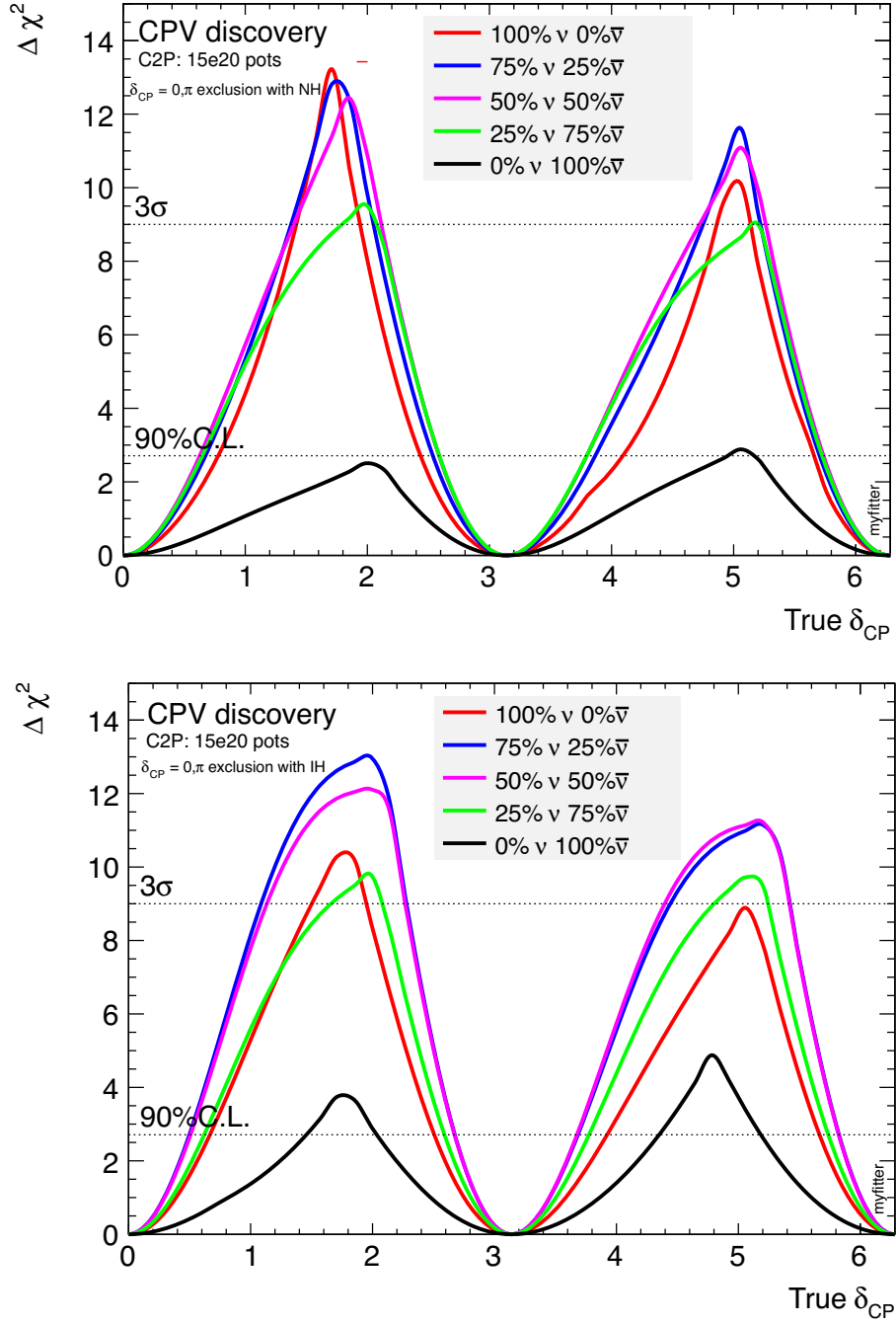
Figure 12: CPV sensitivity for different sharing between $\nu : \bar{\nu}$ running modes, for $1.5 \; 10^{21}$ protons on target and LBNO 20 kton detector. The upper plot is for NH and the lower plot for IH.

significance of our standard method to a first maximum only and a rate only analysis. The study of the significance of the events around the 2nd oscillation maximum was done by evaluating the CPV sensitivity with a cut on the reconstructed energy of the e-like events
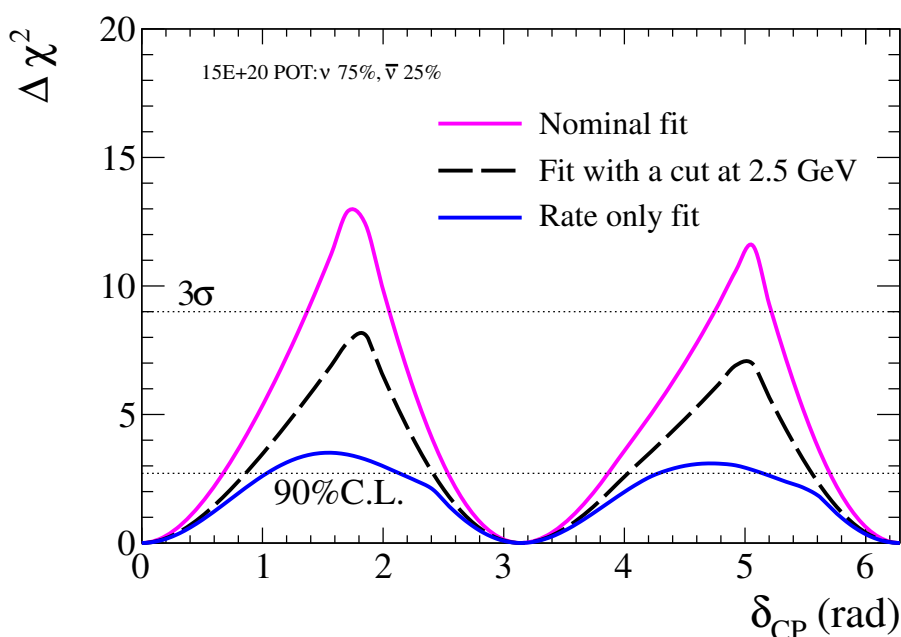
Figure 13: Comparison of the CPV sensitivities of a rate only analysis, an analysis with a cut on a reconstructed energy at 2.5 GeV (excluding the 2nd maximum), and the nominal case where the full event spectrum is used.

placed at 2.5 GeV. This effectively removed all information about the 2nd maximum from the e-like sample. In addition we have tested the importance of performing an analysis based on the e-like event distributions by a rate only analysis evaluation. The rate only measurement leads to a drastic loss of sensitivity of the experiment to the CPV. These studies are shown in figure 13. The important quantity in this plot is the width of the interval below the curve for a given confidence level, which tells us the fraction of unknown parameter space for which we would be able to discover CP violation. As can be seen in this plot, the rate only measurement leads to a drastic loss of sensitivity of the experiment to the CPV. The power of measuring events over an energy range that covers the 1st and the 2nd oscillation maxima is also evident.

9.3 Impact of prior uncertainties on the δ_{CP} discovery potential

The effects of the prior uncertainties on the oscillation parameters have been studied in detail. The CP phase space coverage has been evaluated setting one prior at time for each oscillation parameter according to table 5. This is shown in figure 14 where it is evident that the priors with the largest impact is that on θ_{13}.

In figure 15 we show the effects on the expected electron neutrinos energy spectrum when values of θ_{13} and θ_{23} are varied by $\pm 1\sigma$ for both the appearance and the disappearance channel. This effect is represented by a white band whose binned histograms limits correspond to the reconstructed energy spectrum assuming the minimum and the maximum value of the two mixing angles inside their 1σ range of variability. The statistical
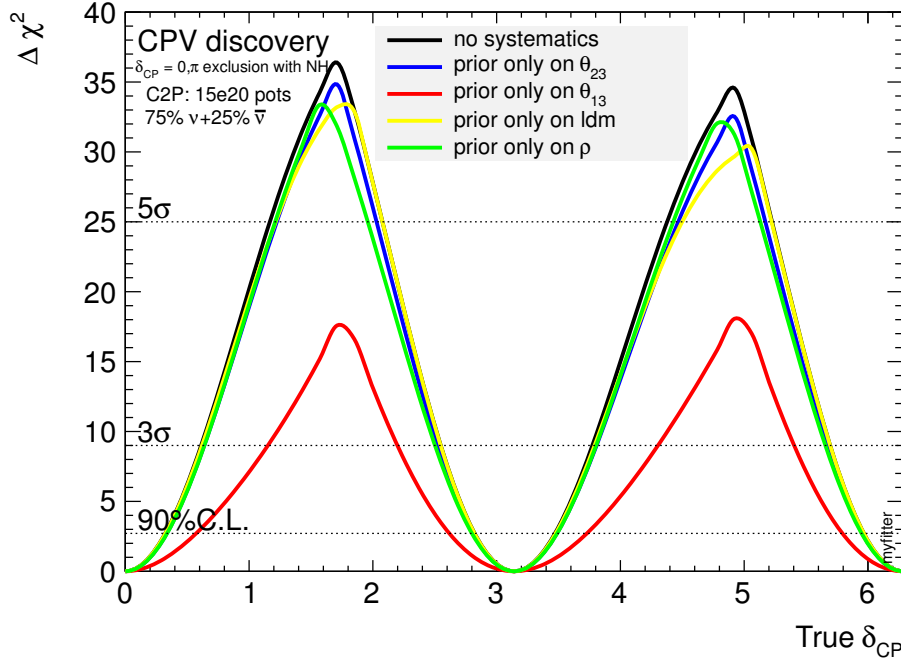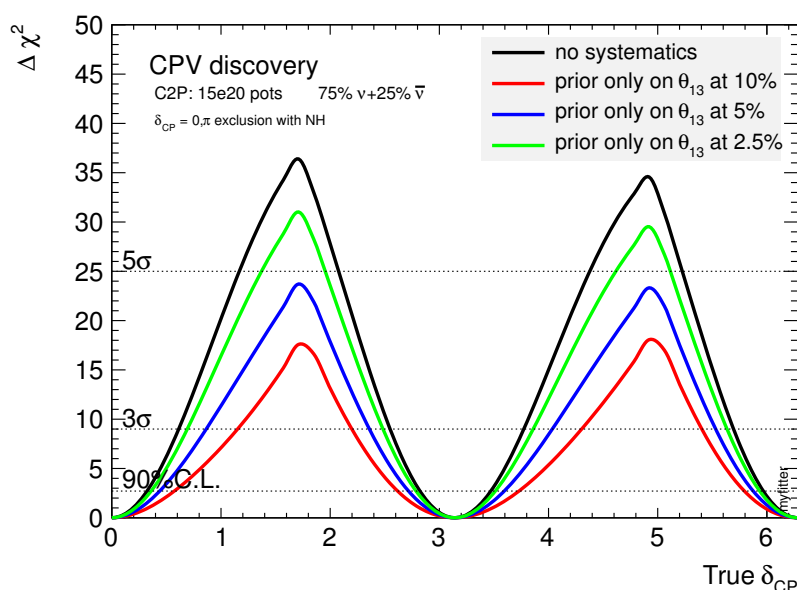
Figure 14: Impact of systematic errors: CPV sensitivity of LBNO phase I as a function of δ_{CP}, with only statistical and no systematic errors (black), and effect of each prior on the oscillation parameters (blue, red, yellow, green).
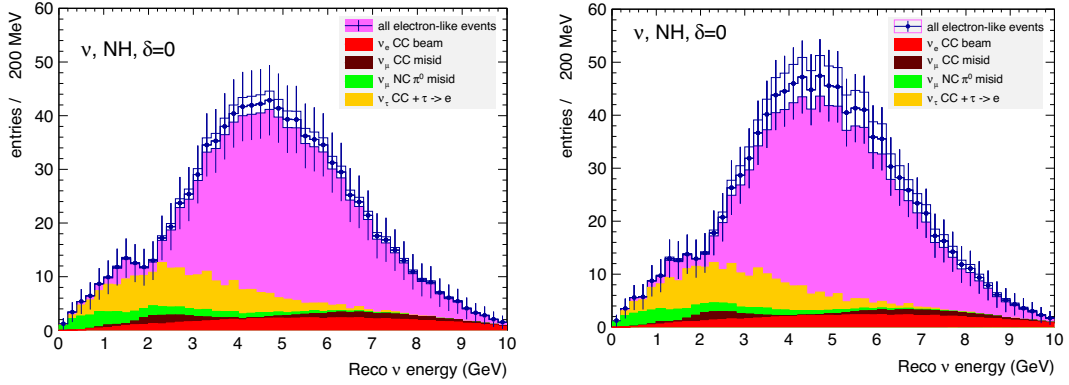
Figure 15: Measured e-like spectrum. Left: maximum and minimum band if $\sin^2 \theta_{23}$ is varied by $\pm 1\sigma$. Right: maximum and minimum band if $\sin^2 2\theta_{13}$ is varied by $\pm 1\sigma$ in the appearance channel.

error for each bin is also shown. We would like to stress the 1σ effect represented by the white band is a fully correlated effect whereas the statistical error is bin-to-bin uncorrelated. Each one of these effects (uncertainty on θ_{13} and θ_{23}) is thus more important than the statistical error in each bin which fluctuates in both directions around the average bin value represented in the histogram.

Figure 16: Impact of systematic errors: CPV sensitivity of LBNO phase I as a function of δ_{CP}, with only statistical and no systematic errors (black), and effect of the error on the $\sin^2 2\theta_{13}$ parameter prior of $\pm 10\%$ (green), $\pm 5\%$ (blue), $\pm 2.5\%$ (red).

9.3.1 Influence of θ_{13} on the δ_{CP} discovery potential

The effect of the knowledge of θ_{13} has been studied in detail. As stated in the previous paragraphs the knowledge of θ_{13} has a very important role on the δ_{CP} discovery potential. It is of great value to reach a more precise measurement of this angle in order to increase the δ_{CP} sensitivity. In figure 16 we show the effect of varying the prior on θ_{13} between 0% and 10% when all the other systematic errors on the oscillation parameters are set to 0%. In figure 17 we show the effect on the δ_{CP} sensitivity with all the systematic errors included. We find that the prior knowledge of θ_{13} is important to constrain δ_{CP}, even in presence of all other systematic errors.

9.3.2 Influence of θ_{23} on the δ_{CP} discovery potential

Now that the value of θ_{13} mixing angle has been measured, the knowledge of the mixing angles which describe the PMNS matrix has changed significantly. Whilst previously θ_{13} was not known, the uncertainty on it had a dominant influence on the possible discovery reach of long-baseline facilities, now it makes sense to investigate also the influence of θ_{23} (excluding δ_{CP}) whose uncertainty has as well a large impact. Its true value influences the sensitivity of CPV as shown in figure 18. We see that variations in θ_{23} induce only slight changes in the sensitivity to δ_{CP} at the 90% CL. At higher significances, the true value of θ_{23} plays a more important role. At the 3σ confidence level, the change in θ_{23} by 1σ can make the difference between having no ability to measure CP violation and being able to exclude CP violation for around 30% of the parameter space.

The dependence of the discovery reach on θ_{23} can be understood analytically by following the method introduced in ref. [36]. This procedure can be modified to account for more
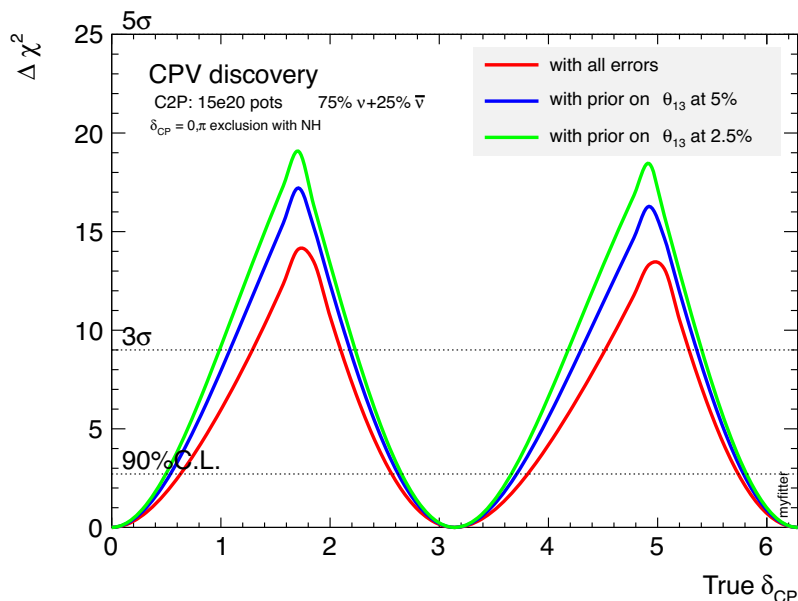
Figure 17: Same as figure 16 but with all other systematic errors included.
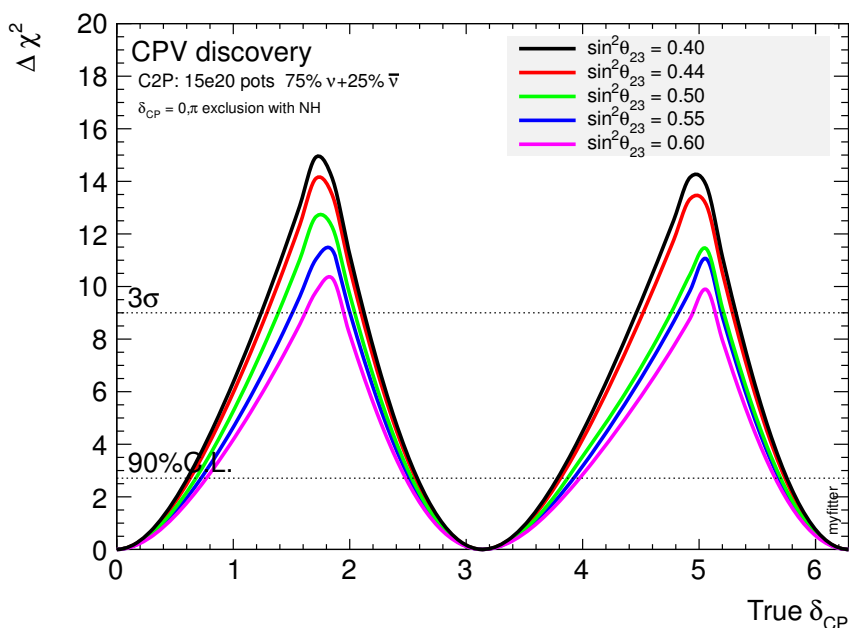
Figure 18: Impact of the prior value of θ_{23}: CPV sensitivity of LBNO phase I as a function of δ_{CP} for a range of values of θ_{23}.

complicated scenarios by combining neutrino and antineutrino running, including matter effects and non-trivial flux profiles; however, for our purposes of extracting the dependence of $\Delta\delta_{CP}$ on θ_{23}, this will not change the functional behaviour and has been omitted for clarity. To find the dependence on θ_{23}, we use the approximate form for the probabilities of the form of eq. (2.2). For the known value of θ_{13}, we can find approximate forms for

the θ_{23} dependence of the probability and its derivative by retaining their leading order behaviour

$$P(\nu_\mu \to \nu_e) \propto \sin^2\theta_{23}, \quad \text{and} \quad \frac{\partial P}{\partial \delta_{\mathrm{CP}}} \propto \sin(2\theta_{23}).$$

Using these two expressions, we can compute the leading order dependence of $\Delta\delta_{\mathrm{CP}}$ on θ_{23} to be

$$\Delta\delta_{\mathrm{CP}} = \frac{\sqrt{P(\nu_\mu \to \nu_e)}}{\frac{\partial P}{\partial \delta_{\mathrm{CP}}}} = C\frac{\sin\theta_{23}}{\sin(2\theta_{23})} \propto \sec\theta_{23}, \tag{9.1}$$

where C is a constant factor. Using eq. (9.1), we can see that the precision to δ_{CP} decreases with increasing θ_{23} within the currently allowed region. In figure 18, $\Delta\delta_{\mathrm{CP}}$ is indicated by the width of the region of good fit around $\delta_{\mathrm{CP}} = 0$ and we can see that this interval grows with increasing θ_{23}. Exact numerical computations confirm the validity of the analytical expression.

### 9.4 Impact of event normalization systematics on the δ_{CP} discovery potential

The impact of systematics due to the knowledge of signal and background normalization has also been studied. Results are shown in figure 19 and 20. In figure 19 the impact of each systematic effect on the δ_{CP} sensitivity is shown: it is evident that the most important systematic error is the one on the signal channel normalization, as could be expected. In figure 20, the variability band due to the effects of systematics is compared to the statistical error for the appearance and disappearance channels. For the disappearance channel the effect is negligible. Errors on normalizations have been considered, very conservatively, to be fully correlated according to table 6. Their effect is smaller than the statistical uncertainty. This study shows also the importance to have a near detector in order to reduce the effect of these uncertainties.

9.5 Statistical power as a function of exposure

The statistical power of LBNO for CPV determination as a function of exposure is shown in figure 21, for the two different CLs of 90% and 3σ. The two most favourable cases, $\delta_{\mathrm{CP}} = \pi/2$ or $3\pi/2$, are considered.

10 Ultimate CPV sensitivity

We have seen that the LBNO Phase I has significant physics goals, in particular it is guaranteed to be fully conclusive for MH discovery with an expected 5σ C.L. over the full range of δ_{CP}. On the other hand, the CPV sensitivity reach is more difficult to predict, since ultimately is dependent on the achievable systematic errors and on the true δ_{CP}. We have chosen to use presently realistic errors on oscillation parameters and on the normalisation of the signal and backgrounds. With the series of expected new measurements and possibly the addition of dedicated measurements from experiments on hadro-production and neutrino cross-sections, it is conceivable to think that the overall balance of errors could be
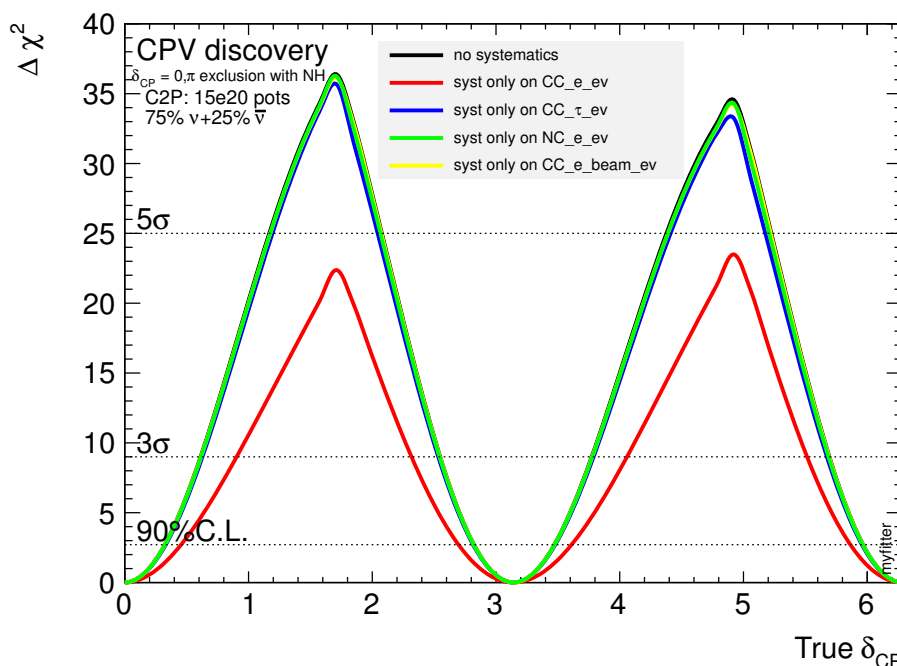
Figure 19: Impact of systematic errors: CPV sensitivity of LBNO phase I as a function of δ_{CP}, with only statistical and no systematic errors (black), and effect of the error on the normalisation of the signal and backgrounds.
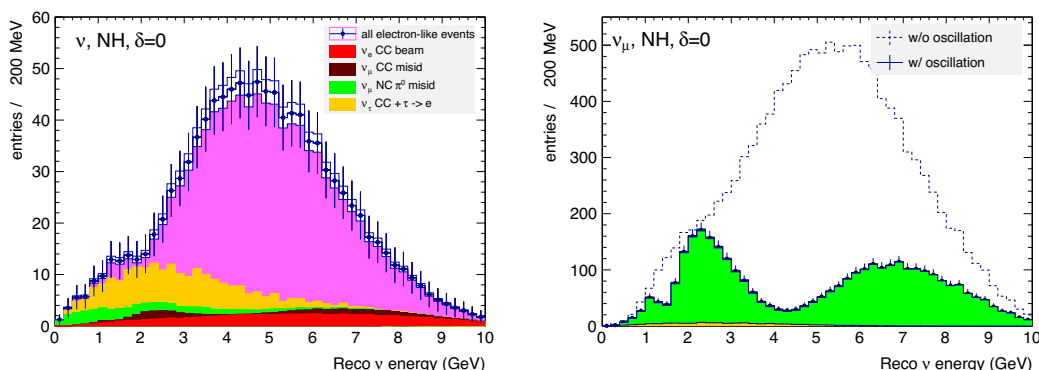
Figure 20: Measured neutrino spectra for (left) e-like appearance (right) muon-like disappearance channels, when all the normalisation errors listed in table 6 are varied by $\pm 1\sigma$ in a fully correlated way. Statistical error are also shown.

reduced in the future, thereby improving further the expected CPV sensitivity of LBNO Phase I. The situation will keep to be monitored, as new experimental results are published.

On the other hand, an alternative method is to increase the detector mass and the neutrino beam power in order to decrease the statistical error around the 2nd oscillation maximum. Because of the natural cut-off of the muon-neutrino flux spectrum at low energy, and the linear increase of the total neutrino cross-section with energy, the 2nd maximum is more difficult to study than the 1st maximum. However, this is still possible at the
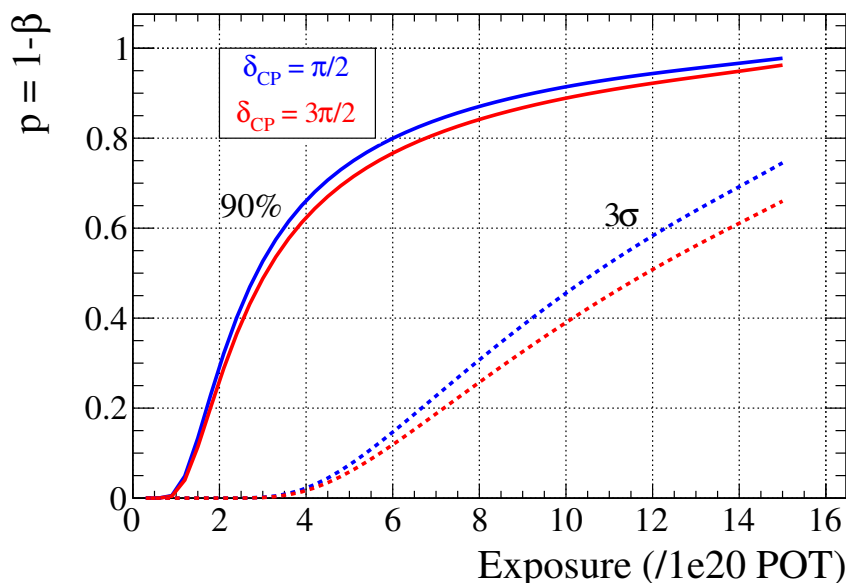
Figure 21: Statistical power for CPV discovery as a function of exposure for 90% and 3σ CL assuming NH. The far detector of 20 kton LAr and 750 kW SPS neutrino beam are assumed. We use the nominal conservative systematic errors (see text).

LBNO baseline of 2300 km since the 2nd maximum is at an accessible energy of $\sim 1.5\,\mathrm{GeV}$. Since the CP-asymmetry at the 2nd maximum is more sensitive to δ_{CP} than at the first maximum, a significant gain is obtained by populating this region with oscillation events. This is one of the main goals of the LBNO Phase II. The expected CPV sensitivity as a function of δ_{CP} is shown in figure 22 for various upgrades of beam power with the HP-PS, and of the far detector mass, from 20 kton to 70 kton. With a new powerful proton driver such as the conceptual HP-PS and a 70 kton detector mass, the coverage at $> 5\sigma$'s C.L. will be $\sim 54\%$ after 10 years.

11 Summary and conclusions

The LBNO experiment is the outcome of intense and comprehensive design studies supported by the European Commission since 2008. In an incremental approach, we propose LBNO with a 20 kton underground detector as the first stage of a new neutrino observatory able to address long-baseline neutrino physics as well as neutrino astrophysics. The programme has a clear long-term vision for future stages of the experiment, including the Neutrino Factory [37], for which the baseline of 2300 km is well adapted.

Unlike the attempts to infer MH with atmospheric neutrinos in multi-megaton low-threshold detectors [38, 39], such as the one proposed with PINGU ([40]; for updated sensitivities, see [41]) or ORCA (for a discussion on the physics potential see e.g. [42]), or with medium-baseline reactor experiments [44], such as JUNO (see e.g. [43]), the accelerator-based approach of LBNO addresses both fundamental problems of CPV and MH in clean
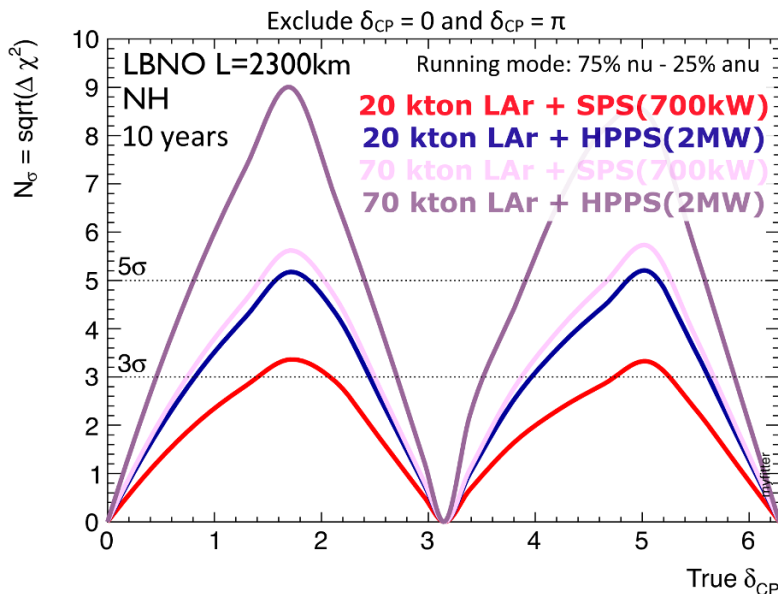
Figure 22: CPV sensitivity as a function of δ_{CP} for various upgrades of beam power with the HP-PS, and of the far detector mass, with 20 kton and 70 kton.

and straightforward conditions, profiting from the ability to reverse the focusing horns polarity and from the well-known and monitored fluxes, which characterise accelerator-based neutrino beams. The mass hierarchy cannot be fully explored by T2K or NOvA [45] given the relatively short baselines of those experiments. As shown in [46] NOvA or a combination of NOvA and T2K can at most reach a 3σ confidence level, assuming the median experiment sensitivity, and only for half of the allowed δ_{CP} values.

In this paper, we have presented our state-of-the-art studies of the expected sensitivity to CPV and MH. We have addressed the impact of the knowledge of the oscillation parameters and of the systematics errors of the experiment. We employed a Monte-Carlo technique simulating a very large number of toy experiments to estimate the confidence level of the MH and CPV measurements. We find that, with the capability of reversing the horn focusing polarity, and even under pessimistic assumptions on systematic errors, LBNO alone provides a direct and guaranteed discovery of MH with $\geq 3\sigma (\geq 5\sigma)$ confidence level, independently of the value of the CP phase and the octant of θ_{23}, within $\sim 2.5(5)$ years of CERN SPS running. The first stage of LBNO will therefore discover the mass hierarchy with certainty.

LBNO has also a unique sensitivity to CPV through the exploration of the first and second oscillation maxima, making possible to study the L/E modulation which should match that expected by δ_{CP} terms in the oscillation probability. With conservative expectations on the systematic errors and after 10 years of CERN SPS running, a significance for CPV above $> 3\sigma$'s C.L. will be reached for $\sim 25(40)\%$ of the δ_{CP} values, under the assumption that $\sin^2 2\theta_{13}$ will be known from reactor experiments with a precision of $\pm 10(2.5)\%$.

The ultimate CPV reach is sensitive to the knowledge of the oscillation parameters and to the assumed flux, cross-section and detector-related systematic errors. The CPV reach

is larger if sources of systematic errors can be controlled below the values conservatively assumed in our present study. In particular, improvements in the present knowledge of differential neutrino interaction cross-sections would increase the expected CPV discovery potential of LBNO. Alternatively, with an increased exposure aimed at increasing the number of oscillated around the 2nd maximum, a CPV discovery level $> 5\sigma$'s C.L. is reachable over a wide range of δ_{CP} values. With a new powerful proton driver such as the conceptual HP-PS and a 70 kton detector mass, the coverage at $> 5\sigma$'s C.L. will be $\sim$54% after 10 years.

We conclude that the control of systematic errors will be the critical challenge for all next generation long-baseline projects such as LBNE, LBNO and Hyper-Kamiokande. This study has presented a comprehensive overview of how experimental uncertainties, together with our limited knowledge of the oscillation parameter space, effects the physics reach of LBNO. Realistic assumptions regarding systematic uncertainties and analysis priors are mandatory in order to develop any new project of this scale.

Acknowledgments

References

[1] A. Stahl et al., *Expression of Interest for a very Longc Baseline Neutrino Oscillation experiment (LBNO)*, CERN-SPSC-2012-021 (2012).

[2] S.K. Agarwalla, T. Li and A. Rubbia, *An incremental approach to unravel the neutrino mass hierarchy and CP-violation with a long-baseline Superbeam for large θ_{13}*, *JHEP* **05** (2012) 154 [arXiv:1109.6526] [INSPIRE].

[3] Z. Maki, M. Nakagawa and S. Sakata, *Remarks on the unified model of elementary particles*, *Prog. Theor. Phys.* **28** (1962) 870 [INSPIRE].

[4] B. Pontecorvo, *Neutrino experiments and the problem of conservation of leptonic charge*, *Sov. Phys. JETP* **26** (1968) 984 [*Zh. Eksp. Teor. Fiz.* **53** (1967) 1717] [INSPIRE].

[5] P. Machado, H. Minakata, H. Nunokawa and R. Zukanovich Funchal, *Combining accelerator and reactor measurements of θ_{13}: the first result*, *JHEP* **05** (2012) 023 [arXiv:1111.3330] [INSPIRE].

[6] G. Fogli, E. Lisi, A. Marrone, D. Montanino, A. Palazzo et al., *Global analysis of neutrino masses, mixings and phases: entering the era of leptonic CP-violation searches*, *Phys. Rev.* **D 86** (2012) 013012 [arXiv:1205.5254] [INSPIRE].

[7] D. Forero, M. Tortola and J. Valle, *Global status of neutrino oscillation parameters after Neutrino-2012*, *Phys. Rev.* **D 86** (2012) 073012 [arXiv:1205.4018] [INSPIRE].

[8] M. Gonzalez-Garcia, M. Maltoni, J. Salvado and T. Schwetz, *Global fit to three neutrino mixing: critical look at present precision*, *JHEP* **12** (2012) 123 [arXiv:1209.3023] [INSPIRE].

[9] F. Piquemal, *Reactor neutrinos, double beta and beta decays experimental review*, PoS(ICHEP 2010)553.

[10] L. Wolfenstein, *Neutrino oscillations in matter*, *Phys. Rev.* **D 17** (1978) 2369 [INSPIRE].

[11] J. Arafune, M. Koike and J. Sato, *CP violation and matter effect in long baseline neutrino oscillation experiments*, *Phys. Rev.* **D 56** (1997) 3093 [*Erratum ibid.* **D 60** (1999) 119905] [hep-ph/9703351] [INSPIRE].

[12] V. Barger, D. Marfatia and K. Whisnant, *Breaking eight fold degeneracies in neutrino CP-violation, mixing and mass hierarchy*, *Phys. Rev.* **D 65** (2002) 073023 [hep-ph/0112119] [INSPIRE].

[13] LBNE collaboration, C. Adams et al., *Scientific opportunities with the long-baseline neutrino experiment*, arXiv:1307.7335 [INSPIRE].

[14] K. Abe et al., *Letter of intent: the Hyper-Kamiokande experiment — detector design and physics potential*, arXiv:1109.3262 [INSPIRE].

[15] T2K collaboration, K. Abe et al., *The T2K neutrino flux prediction*, *Phys. Rev.* **D 87** (2013) 012001 [arXiv:1211.0469] [INSPIRE].

[16] C. Rubbia, *The liquid argon time projection chamber: a new concept for neutrino detectors*, CERN-EP-INT-77-08 (1977).

[17] A. Rubbia, *Experiments for CP-violation: a giant liquid argon scintillation, Cerenkov and charge imaging experiment?*, hep-ph/0402110 [INSPIRE].

[18] A. Rubbia et al., *Underground neutrino detectors for particle and astroparticle science: the Giant Liquid Argon Charge Imaging ExpeRiment (GLACIER)*, *J. Phys. Conf. Ser.* **171** (2009) 012020 [arXiv:0908.1286] [INSPIRE].

[19] ISS DETECTOR WORKING GROUP collaboration, T. Abe et al., *Detectors and flux instrumentation for future neutrino facilities*, 2009 *JINST* **4** T05001 [arXiv:0712.4129] [INSPIRE].

[20] A. Cervera, A. Laing, J. Martin-Albo and F. Soler, *Performance of the MIND detector at a Neutrino Factory using realistic muon reconstruction*, *Nucl. Instrum. Meth.* **A 624** (2010) 601 [arXiv:1004.0358] [INSPIRE].

[21] A. Rubbia, *A CERN-based high-intensity high-energy proton source for long baseline neutrino oscillation experiments with next-generation large underground detectors for proton decay searches and neutrino physics and astrophysics*, arXiv:1003.1921 [INSPIRE].

[22] T2K collaboration, K. Abe et al., *Indication of electron neutrino appearance from an accelerator-produced off-axis muon neutrino beam*, *Phys. Rev. Lett.* **107** (2011) 041801 [arXiv:1106.2822] [INSPIRE].

[23] DAYA-BAY collaboration, F. An et al., *Observation of electron-antineutrino disappearance at Daya Bay*, *Phys. Rev. Lett.* **108** (2012) 171803 [`arXiv:1203.1669`] [INSPIRE].

[24] T2K collaboration, K. Abe et al., *Evidence of electron neutrino appearance in a muon neutrino beam*, *Phys. Rev.* **D 88** (2013) 032002 [`arXiv:1304.0841`] [INSPIRE].

[25] T2K collaboration, K. Abe et al., *Observation of electron neutrino appearance in a muon neutrino beam*, *Phys. Rev. Lett.* **112** (2014) 061802 [`arXiv:1311.4750`] [INSPIRE].

[26] K. Elsener et al., *The CERN Neutrino beam to Gran Sasso (NGS): conceptual technical design*, CERN, Switzerland (1998).

[27] E. Shaposhnikova et al., *Recent intensity increase in the CERN accelerator chain*, CERN-AB-2005-029 (2005).

[28] B. Goddard et al., *Chamonix 2012 workshop on LHC performance*, CERN-ATS-2012-069 (2012).

[29] Y. Papaphilippou et al., *Design options of a high-power proton synchrotron for LAGUNA-LBNO*, in the proceedings of the 4th *International Particle Accelerator Conference (IPAC13)*, May 12–17, Shangai, China (2013).

[30] B. Goddard et al., *Non-local Fast Extraction from the CERN SPS at 100 and 440 GeV*, in the proceedings of the 4th *International Particle Accelerator Conference (IPAC13)*, May 12–17, Shangai, China (2013).

[31] V. Papadimitriou, *Status of the LBNE Neutrino Beamline*, `arXiv:1112.0720` [INSPIRE].

[32] X. Qian et al., *Statistical evaluation of experimental determinations of neutrino mass hierarchy*, *Phys. Rev.* **D 86** (2012) 113011 [`arXiv:1210.3651`] [INSPIRE].

[33] S.-F. Ge, K. Hagiwara, N. Okamura and Y. Takaesu, *Determination of mass hierarchy with medium baseline reactor neutrino experiments*, *JHEP* **05** (2013) 131 [`arXiv:1210.8141`] [INSPIRE].

[34] M. Blennow, P. Coloma, P. Huber and T. Schwetz, *Quantifying the sensitivity of oscillation experiments to the neutrino mass ordering*, *JHEP* **03** (2014) 028 [`arXiv:1311.1822`] [INSPIRE].

[35] A.M. Dziewonski and D.L. Anderson, *Preliminary reference earth model*, *Phys. Earth Planet. Interiors* **25** (1981) 297 [INSPIRE].

[36] P. Coloma et al., *Precision on leptonic mixing parameters at future neutrino oscillation experiments*, *JHEP* **06** (2012) 073 [`arXiv:1203.5651`] [INSPIRE].

[37] T. Edgecock et al., *High intensity neutrino oscillation facilities in Europe*, *Phys. Rev. ST Accel. Beams* **16** (2013) 021002 [`arXiv:1305.4067`] [INSPIRE].

[38] M. Ribordy and A.Y. Smirnov, *Improving the neutrino mass hierarchy identification with inelasticity measurement in PINGU and ORCA*, *Phys. Rev.* **D 87** (2013) 113007 [`arXiv:1303.0758`] [INSPIRE].

[39] D. Franco et al., *Mass hierarchy discrimination with atmospheric neutrinos in large volume ice/water Cherenkov detectors*, *JHEP* **04** (2013) 008 [`arXiv:1301.4332`] [INSPIRE].

[40] IceCube, PINGU collaboration, M. Aartsen et al., *PINGU sensitivity to the neutrino mass hierarchy*, `arXiv:1306.5846` [INSPIRE].

[41] D. Cohen, *PINGU and the Neutrino Mass Hierarchy*, talk given at the *P5 Workshop on the Future of High Energy Physics*, December 15–18, Brookhaven National Laboratory, Upton, U.S.A. (2013).

[42] KM3NeT collaboration, P. Kooijman, *ORCA status report*, talk given at the 33rd International Conference of Cosmic Rays (IRC2013), July 2–9, Rio de Janeiro, Brazil (2013).

[43] Y.-F. Li, J. Cao, Y. Wang and L. Zhan, *Unambiguous determination of the neutrino mass hierarchy using reactor neutrinos*, *Phys. Rev.* **D 88** (2013) 013008 [`arXiv:1303.6733`] [ɪɴSPIRE].

[44] A. Balantekin et al., *Neutrino mass hierarchy determination and other physics potential of medium-baseline reactor neutrino oscillation experiments*, `arXiv:1307.7419` [ɪɴSPIRE].

[45] NOvA collaboration, D. Ayres et al., *NOvA: Proposal to build a 30 kiloton off-axis detector to study $\nu_\mu \to \nu_e$ oscillations in the NuMI beamline*, `hep-ex/0503053` [ɪɴSPIRE].

[46] NOvA collaboration, R. Patterson, *The NOvA experiment: status and outlook*, *Nucl. Phys. Proc. Suppl.* **235-236** (2013) 151 [`arXiv:1209.0716`] [ɪɴSPIRE].